MOLECULAR LASERS IN E-BEAM STABILIZED DISCHARGED

S. R. Byron, et al

Mathematical Sciences Northwest, Incorporated

Prepared for:

Office of Naval Research

August 1974

UNCLASSIFIED

SECURITY CLASSIFICATION OF THIS PAGE (When Data Entered)

REPORT DOCUMENTATION PAGE

READ INSTRUCTIONS BEFORE COMPLETING FORM

1. REPORT NUMBER: 74-105-3	2. GOVT ACCESSION NO.
3. RECIPIENT'S CATALOG NUMBER: AD/A-001062	
4. TITLE (and Subtitle): MOLECULAR LASERS IN E-BEAM STABILIZED DISCHARGES	5. TYPE OF REPORT & PERIOD COVERED: Semi-Annual #3, 15 May 1973-15 Nov. 1973
	6. PERFORMING ORG. REPORT NUMBER
7. AUTHOR(s): S. R. Byron, L. Y. Nelson, C. H. Fisher, G. J. Mullaney, and A. L. Pindroh	8. CONTRACT OR GRANT NUMBER(s): N00014-72-C-0430
9. PERFORMING ORGANIZATION NAME AND ADDRESS: Mathematical Sciences Northwest, Inc., 3030 N. E. 45th Street, Seattle, Washington, 98105	10. PROGRAM ELEMENT, PROJECT, TASK AREA & WORK UNIT NUMBERS: Pro.Ele.62301E; Proj.4E90, Task Area 1807; Work Unit 01C-408
11. CONTROLLING OFFICE NAME AND ADDRESS: Office of Naval Research, 800 North Quincy Street, Arlington, VA 22217	12. REPORT DATE: August 1974
	13. NUMBER OF PAGES: 67
14. MONITORING AGENCY NAME & ADDRESS(if different from Controlling Office)	15. SECURITY CLASS. (of this report): UNCLASSIFIED
	15a. DECLASSIFICATION/DOWNGRADING SCHEDULE

16. DISTRIBUTION STATEMENT (of this Report)

17. DISTRIBUTION STATEMENT (of the abstract entered in Block 20, if different from Report)

18. SUPPLEMENTARY NOTES

19. KEY WORDS (Continue on reverse side if necessary and identify by block number)

HF/DF Lasers
Electron Beam
Electronic State Lasers
N_2 Visible Lasers

20. ABSTRACT (Continue on reverse side if necessary and identify by block number)

This program is directed toward developing efficient, high energy density electric discharge lasers in the infrared and visible regions of the spectrum. A high current, electron-beam-stabilized, electric discharge is used for excitation. Infrared laser emission and absorption from the vibrational levels of HF (2.8 to 3.1 μm) and DF (3.8 to 4.1 μm) in various gas mixtures is being studied to determine laser efficiency and to obtain a detailed model of the vibrational kinetics. The efficiency of electric discharge excitation of molecular vibration in these gases is being determined by solving the electron

DD FORM 1 JAN 73 1473 EDITION OF 1 NOV 65 IS OBSOLETE

UNCLASSIFIED

SECURITY CLASSIFICATION OF THIS PAGE (When Data Entered)

ABSTRACT

This program is directed toward developing efficient, high energy density electric discharge lasers in the infrared and visible regions of the spectrum. A high current, electron-beam-stabilized, electric discharge is used for excitation. Infrared laser emission and absorption from the vibrational levels of HF (2.8 to 3.1 μm) and DF (3.8 to 4.1 μm) in various gas mixtures is being studied to determine laser efficiency and to obtain a detailed model of the vibrational kinetics. The efficiency of electric discharge excitation of molecular vibration in these gases is being determined by solving the electron Boltzmann equation. Electronic state excitation by e-beam stabilized electric discharges in N_2 and other molecular systems is being investigated in an effort to develop efficient, long pulse visible lasers.

20. Abstract continued

Boltzmann equation. Electronic state excitation by e-beam stabilized electric discharges in N_2 and other molecular systems is being investigated in an effort to develop efficient, long pulse visible lasers.

MOLECULAR LASERS IN E-BEAM STABILIZED DISCHARGES

Semi-Annual Technical Report No. 3
Covering the Period
15 May 1973 to 15 November 1973

By

S. R. Byron, L. Y. Nelson, C. H. Fisher,
C. J. Mullaney, and A. L. Pindroh

Mathematical Sciences Northwest, Inc.
4545 Fifteenth Avenue N. E.
Seattle, Washington 98105

June 1974

Contract N00014-72-C-0430

Sponsored by

Advanced Research Projects Agency
ARPA Order No. 1807

Monitored by

Office of Naval Research
Code 421

ARPA ORDER NO.:	1807
PROGRAM CODE:	2E90
NAME OF CONTRACTOR:	Mathematical Sciences Northwest, Inc.
EFFECTIVE DATE OF CONTRACT:	15 March 1972 through 30 June 1974
CONTRACT AMOUNT:	$535,567
CONTRACT NUMBER:	N00014-72-C-0430
PRINCIPAL INVESTIGATOR:	Dr. S. R. Byron (206)524-9300
SCIENTIFIC OFFICER:	Director, Physics Programs Physical Sciences Division Office of Naval Research Department of the Navy 800 North Quincy Street Arlington, Virginia 22217
DISCLAIMER:	The views and conclusions contained in this document are those of the authors and should not be interpreted as necessarily representing the official policies, either expressed or implied, of the Advanced Research Projects Agency or the U. S. Government.

TABLE OF CONTENTS

SECTION		PAGE
I	SUMMARY	1
	1.1. HF and DF Laser Studies	1
	1.2. Electronic State Lasers	2
	1.3. Uniformity of the 5-Tube Plasma Diode Electron Gun	4
II	HF AND DF LASER EXPERIMENTS	5
	2.1. Ar/DF and Ar/D_2/DF Laser Cavity Measurements	5
	2.2. Rotational Equilibration in HF Gas Mixtures	8
	2.3. Laser Output Energy Measurements in HF Gas Mixtures	13
	2.4. Chemical Laser Output Observed with Ar/H_2/SF_6 Mixtures	14
III	HF KINETICS MEASUREMENTS AND ANALYSIS	17
	3.1. HF Probe Laser Absorption Measurement Technique	17
	3.2. Probe Laser Absorption Measurements of HF Vibrational Decay	21
	3.2.1. Ar/N_2/HF Mixtures	22
	3.2.2. Ar/HF Mixtures	25
	3.2.3. Ar/H_2/HF Mixtures	25
	3.3. Comparison of Computer Model with HF Probe Laser Absorption Measurements	27
	3.3.1. Ar/N_2/HF Excitation Processes	27
	3.3.2. Comparison of Computer Model with Absorption Measurements in Ar/H_2/HF Mixtures	33
IV	ELECTRONIC STATE LASERS: FURTHER STUDY OF THE FIRST POSITIVE AND SECOND POSITIVE BAND SYSTEMS OF N_2	37
	4.1. Experimental Set-Up	37
	4.2. Fluorescence Studies	38
	4.3. Effect of SF_6	47
	4.4. Vibrational Quenching of Lower Level	49
	4.5. Laser Cavity Measurements	51
	4.6. Conclusions	52

Page

REFERENCES 54

APPENDIX A 55

LIST OF TABLES

TABLE		PAGE
I	Time Resolved Spectroscopic Measurements of the Vibration Rotation Lines Observed in HF and DF Electric Discharge Lasers (Gas Pressure, 200 torr; time in μsec is given in parentheses)	6
II	Spectroscopic Measurements of Chemical Laser Emission in $Ar/H_2/SF_6$ Mixtures	15
III	Summary of H_2/HF V-V and V-T Rate Data	23
IV	Ar + N_2 Excited State Reactions	46

LIST OF FIGURES

FIGURE		PAGE
1	Time Sequence of Laser Emission from $Ar/D_2/DF$ Mixtures at 200 Torr. The Discharge Voltage Sensitivity is 700 V/Div and the Discharge Current Sensitivity is 1380 A/Div	7
2	Time Sequence of Laser Emission from $Ar/N_2/HF$ Mixtures at 200 Torr. Voltage and Current Sensitivities Same as Figure 1	9
3	HF Laser Cavity Intensity in Ar/N_2 and $Ar/He/N_2$ Mixtures at 200 Torr, Using 0.4 Percent HF	10
4	Peak Laser Cavity Intensity in $Ar/N_2/HF$ and $Ar/He/N_2/HF$ Mixtures at 200 Torr, Using E/N Values of 0.7 to 1.0 x 10^{-16} V-cm^2	11
5	HF Laser Emission on All Lines from $Ar/H_2/SF_6$ Gas Mixtures at 200 Torr Pumped Directly by External Electron Beam Excitation Alone	15
6	Optical Arrangement Used for HF Probe Laser Absorption and Gain Measurements	18
7	Calculation of HF($v = 0 \rightarrow 1$) Transmission at 300°K and 200 Torr, Heavily Diluted with Ar, Over a Path Length of 82 cm	20
8	Probe Laser Absorption Measurements of HF($v = 1$) Decay Following a 30 µsec Electric Discharge Pulse in 89/10/0.3 Mixtures of $Ar/N_2/HF$ at 200 Torr	24
9	Probe Laser Absorption Measurements of HF($v = 1$) Decay Following a 30 µsec Electric Discharge Pulse in 99.8/0.2 Ar/HF Mixtures at 200 Torr	26
10	Probe Laser Measurements for a 50 µsec Discharge Pulse in 89/10/0.4 $Ar/N_2/HF$ Mixtures at 200 Torr	28

FIGURE		PAGE
11	Measured HF Fraction in v = 1 and v = 2 in 89/10/9.4 $Ar/N_2/HF$ Mixtures at 200 Torr Obtained from Data of Figure 9	30
12	Computer Model Calculations of Optical Gain or Absorption on the 2 → 1 P(7) Transition of HF in 89/10/9.4 Mixtures of $Ar/N_2/HF$ at 200 Torr for a Power Input of 3 kW/cm^3.	32
13	Comparison of Probe Laser Absorption Measurements with Computer Model Results in 89/10/0.3 $Ar/H_2/HF$ Mixtures at 200 Torr and a Power Input of 1.6 kW/cm^3 for 30 μsec	34
14	Time History of the Nitrogen C → B (3370 Å) and B → A (1.04 μm) Fluorescence Produced a) by the E-Beam Stabilized Electric Discharge in an Ar/15% N_2 Mixture at 200 Torr Total Pressure	40
15	Time Decay of the 3370 Å and 1 μ Emission After the Discharge is Terminated for an Ar/15% N_2 Mixture at 200 Torr Total Pressure	42
16	Plot of the Reciprocal of the Square Root of the N_2 First and Second Positive Intensities Versus Time After the Discharge Crowbar	44
17	Effect of Approximately 0.1% SF_6 Addition on the Discharge Voltage, Discharge Current, and 3370 Å Emission for an 85/15 Ar/N_2 Mixture	48
18	Electron Beam Nonuniformities Measured Below the Foil and Screen of the 5-Tube Plasma Diode Electron Gun	55

SECTION I

SUMMARY

1.1. HF and DF Laser Studies

During this reporting period, laser emission has been achieved in DF gas mixtures using electron impact excitation in e-beam stabilized electric discharges. Laser oscillation was observed in Ar/DF and $Ar/D_2/DF$ mixtures on the $2 \rightarrow 1$, $3 \rightarrow 2$, and $4 \rightarrow 3$ bands ranging in wavelength from 3.8 to 4.2 μm. The use of N_2 in the gas mixture eliminated laser emission from DF, contrary to the beneficial effect of N_2 on HF laser emission reported previously.

The use of helium rather than argon as a diluent in HF laser mixtures was found to produce higher laser cavity intensity at a given discharge current and voltage, indicating the possible beneficial effect of faster rotational equilibration. However, with helium as a diluent, the e-beam current required to achieve a given discharge current is significantly higher than that required when argon diluent is used.

Laser output energy was measured for several HF gas mixtures and yielded unexpectedly low results. The highest output energy obtained in a 30 μsec duration pulse was 11 millijoules and corresponded to only 0.06 percent efficiency and 0.3 J/ℓ-atm. This laser output is one to two orders of magnitude less than expected on the basis of the computer model using currently available rate data. This result may be due either to the non-uniformities associated with the 5-tube plasma diode electron

gun or to a significant error in the kinetic modelling data now in general use. A uniform electron gun is being constructed, and probe laser measurements of gain and absorption have been started to provide further data for evaluation of the kinetic model.

The probe laser measurements, taken on several P-branch lines of the 2 → 1 and 3 → 2 bands of HF, showed first that there is no significant V-V exchange process between N_2 and HF. Thus, the laser emission observed in $Ar/N_2/HF$ mixtures arises wholly from electron impact excitation of HF. The apparent electron-energy-averaged cross-section for this process is about 3×10^{-17} cm^2, which is comparable with the cross-section for H_2 vibrational excitation. Additional probe laser data, obtained for $Ar/H_2/HF$ mixtures, showed a very long decay time following termination of the discharge, and indicated the expected effect of V-V transfer from H_2 to HF. However, a comparison with the results of kinetic model computations (which included direct electron impact excitation of HF) showed significant differences, both during the pulse and during the long duration decay. These measurements will be repeated in the uniform discharge chamber now being constructed.

1.2. Electronic State Lasers

Time resolved measurements of N_2 first and second positive band emission in e-beam stabilized discharges showed evidence of three distinct excitation mechanisms. Direct excitation by the external e-beam current was seen, direct excitation by the electric discharge was observed, and

an indirect excitation process was seen which lasted several microseconds following termination of the applied discharge voltage. By analyzing the decay curves, the observed indirect excitation mechanism has been identified with the $N_2(A)$ energy pooling process in which two $N_2(A^3\Sigma_u^+)$ molecules collide to produce a molecule in a higher excited state, plus a ground state molecule.

The effect of SF_6 and C_2H_6 additives on the discharge properties and on the N_2 fluorescence emission was also studied. The addition of 0.1 percent SF_6 cut the discharge current by a factor of about 10, but permitted the application of a correspondingly higher value of E/N. This produced a higher rate of excitation of the C and B states by direct electric discharge processes. and resulted in a 10-fold increase in the ratio of the C state population to the B state population. The addition of C_2H_6 was examined for its potential role as a catalyst to depopulate the vibrationally excited levels of the $N_2(A^3\Sigma_u^+)$ state and thereby speed up the collisional quenching rate of the $N_2(B^3\pi_g)$ state. However, no change in the ratio of $N_2(C)$ emission to $N_2(B)$ emission was seen with the addition of C_2H_6. On the other hand, the indirect excitation mechanism for the B and C states decreased markedly with the addition of C_2H_6.

Laser cavity tests were conducted in N_2/Ar and N_2/He mixtures, with and without SF_6 or C_2H_6 additives, using mirror pairs coated for 3371 Å, 3650 Å, and 1 μm, but with no success.

1.3. Uniformity of the 5-Tube Plasma Diode Electron Gun

The variation in electron beam current density through the foil for the 5-tube plasma diode was measured using an array of current probes. The ratio of the maximum current to the minimum current was found to be about 2, indicating the need for a more uniform electron gun.

SECTION II

HF AND DF LASER EXPERIMENTS

2.1. Ar/DF and Ar/D_2/DF Laser Cavity Measurements

Using the 5-tube plasma diode electron beam and electric discharge chamber described previously (Ref. 1), laser emission in Ar/DF and Ar/D_2/DF was observed at wavelengths from 3.8 to 4.2 μm. The experimental conditions were analogous to those found successful in producing HF laser emission in Ar/HF and Ar/H_2/HF mixtures. The total gas pressure used was 200 torr, and the DF mole fraction was approximately 0.4 percent.

As with the Ar/HF laser, the value of E/N used in Ar/DF mixtures was only 0.1 to 0.2 x 10^{-16} V-cm^2 and the average discharge current density was about 4 A/cm^2. The observed wavelengths and onset and termination times are given in Table I. The observed laser emission from Ar/DF provides further experimental confirmation of direct electron impact excitation of HF and DF vibration.

Laser emission was also observed in mixtures of Ar/D_2/DF (92/7/0.4) using experimental conditions similar to those used previously for Ar/H_2/HF (Ref. 1). The optimum E/N was 0.4 x 10^{-16} V-cm^2 and a maximum average discharge current of 12 A/cm^2 was used. The observed wavelengths and onset and termination times are given in Table I, along with prior results for HF gas mixtures. Typical oscilloscope traces of DF(3 → 2) laser emission on several rotational lines are shown in Figure 1. It is apparent that maximum laser

Table 1. Time Resolved Spectroscopic Measurements of the Vibration Rotation Lines Observed in HF and DF Electric Discharge Lasers (Gas Pressure, 200 torr; time in μsec is given in parentheses).

Transition		Wavelength, μm	Gas Mixture				Wavelength, μm	Gas Mixture	
V	P(J)	HF	Ar/HF	$Ar/H_2/HF$	$Ar/N_2/HF$	N_2/HF	DF	Ar/DF	$Ar/D_2/DF$
1-0	9	2.823			(25-57)		-		
2-1	7	2.870	(10-32)		(6-44)	(12-28)	-		
	8	2.911	(12-40)	(8 -22)	(8-66)		-		
	9	2.954		(11-32)			3.837	(17-43)	
	10	2.999		(22-38)			3.876	(17-42)	
	13	-					3.999		(27-36)
3-2	6	2.964	(9-13)		(6- 9)		-		
	7	3.005	(10-28)	(10-18)	(7-45)		-		
	8	3.048		(10-27)	(32-48)		3.927	(15-24)	
	9	3.094		(24-32)			3.965	(15-46)	
	11	-					4.046		(15-30)
	12	-					4.089		(20-36)
	13	-					4.134		(32-38)
4-3	10	-					4.141		(15-25)
	11	-					4.184		(19-34)

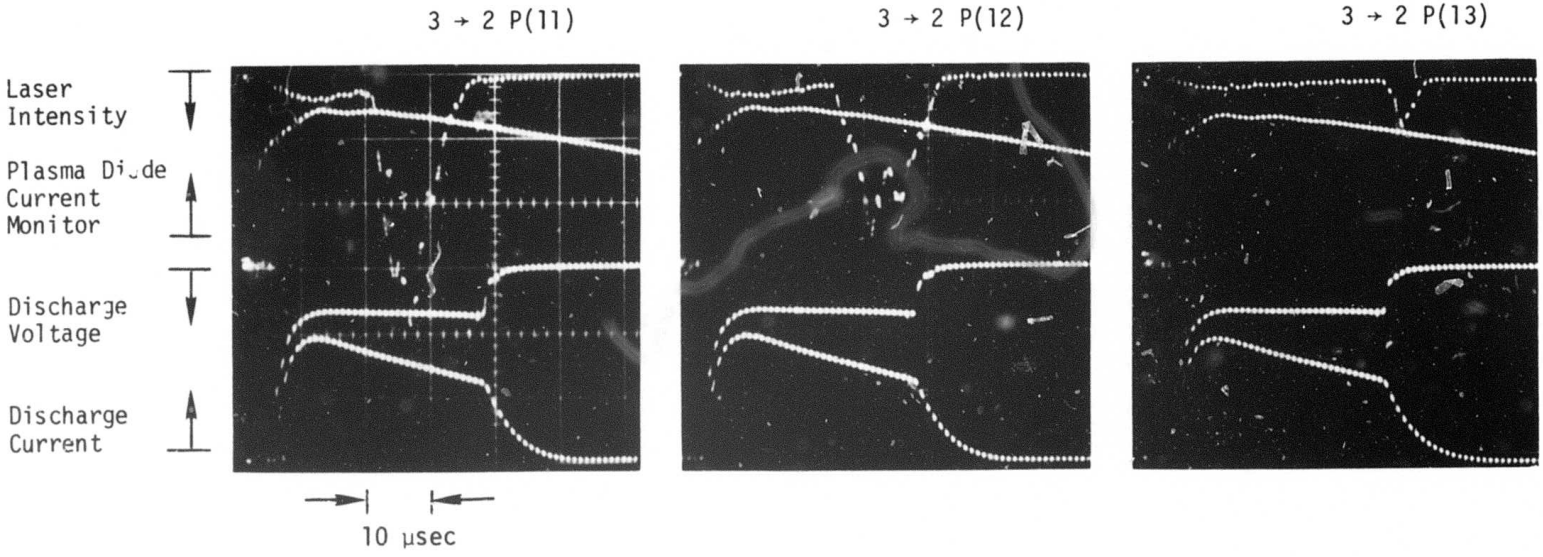

Figure 1. Time Sequence of Laser Emission from $Ar/D_2/DF$ Mixtures at 200 Torr. The Discharge Voltage Sensitivity is 700 V/Div and the Discharge Current Sensitivity is 1380 A/Div.

emission occurs sequentially at increasing J-values throughout the pulse. This observation indicates significant gas heating and partial equilibration of rotational populations by collisional processes. By contrast, the observed time sequence in $Ar/N_2/HF$ mixtures, illustrated in Figure 2, shows strong laser emission simultaneously on adjacent rotational lines, indicating considerably less collisional equilibration of HF rotation in the $Ar/N_2/HF$ mixture. The problem of rotational equilibration in HF laser mixtures is discussed further in Section 2.2 and in Section 3.

Addition of only 3 percent O_2 to an Ar/DF laser mixture completely quenched DF laser emission. When an 89/10/0.3 mixture of $Ar/N_2/DF$ was used, the HF isotopic impurity in the DF supply (about 10 percent) produced laser emission at 2.9 μm, but no laser emission from DF was found. These measurements confirm the detrimental role of O_2 and N_2 on the DF laser (due to rapid vibrational quenching of DF by O_2 and N_2), and illustrate the importance of careful gas preparation and purification.

The DF laser emission observed in these experiments was achieved by eliminating the use of pre-mixed Ar/D_2 gas stored in conventional mild steel gas bottles. Flowmeters connected directly to the pre-purified argon and deuterium gas tanks by polyethylene tubing permitted mixing of the gases as they were flowing into the discharge chamber. This arrangement apparently yielded better gas purity than was achieved with the procedures used previously for pre-mixing Ar/D_2 samples.

2.2. Rotational Equilibration in HF Gas Mixtures

The effect of helium on the total HF laser intensity in a high-Q cavity is shown in Figures 3 and 4. As seen by comparing Figure 3(a)

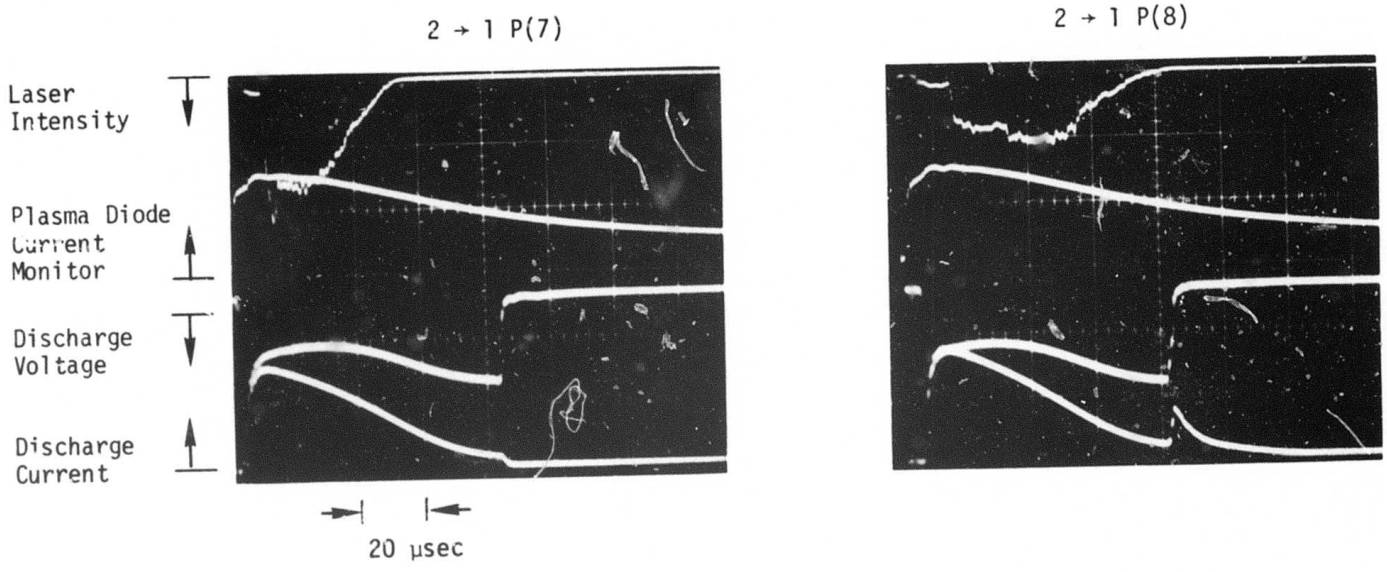

Figure 2. Time Sequence of Laser Emission from $Ar/N_2/HF$ Mixtures at 200 Torr. Voltage and Current Sensitivities Same as Figure 1.

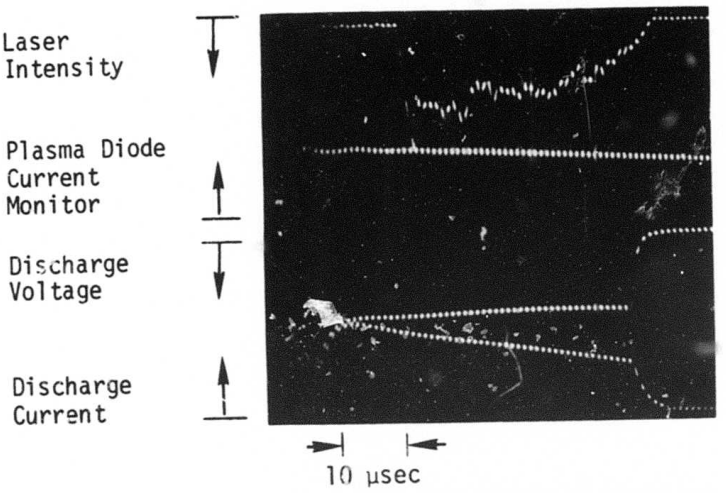

(a)

90/10 Ar/N_2

AT LOW DISCHARGE CURRENT

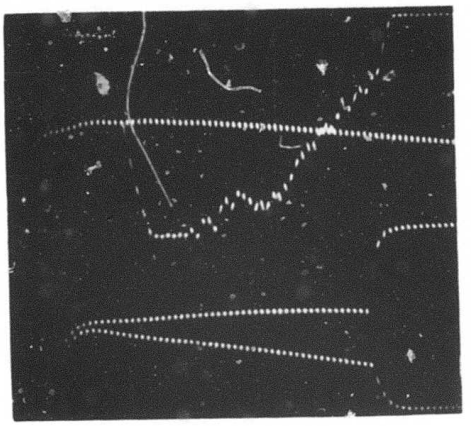

(b)

45/45/10 $Ar/He/N_2$

AT LOW DISCHARGE CURRENT

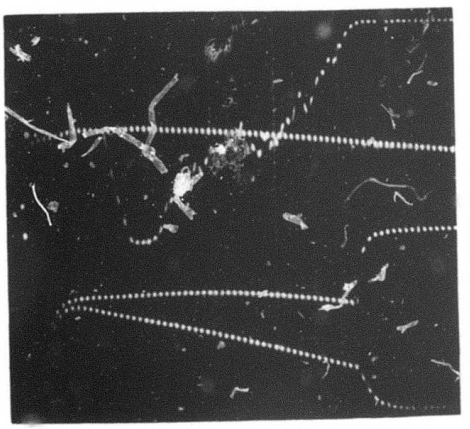

(c)

90/10 Ar/N_2

AT HIGH DISCHARGE CURRENT

Figure 3. HF Laser Cavity Intensity in Ar/N_2 and $Ar/He/N_2$ Mixtures at 200 Torr, Using 0.4 Percent HF

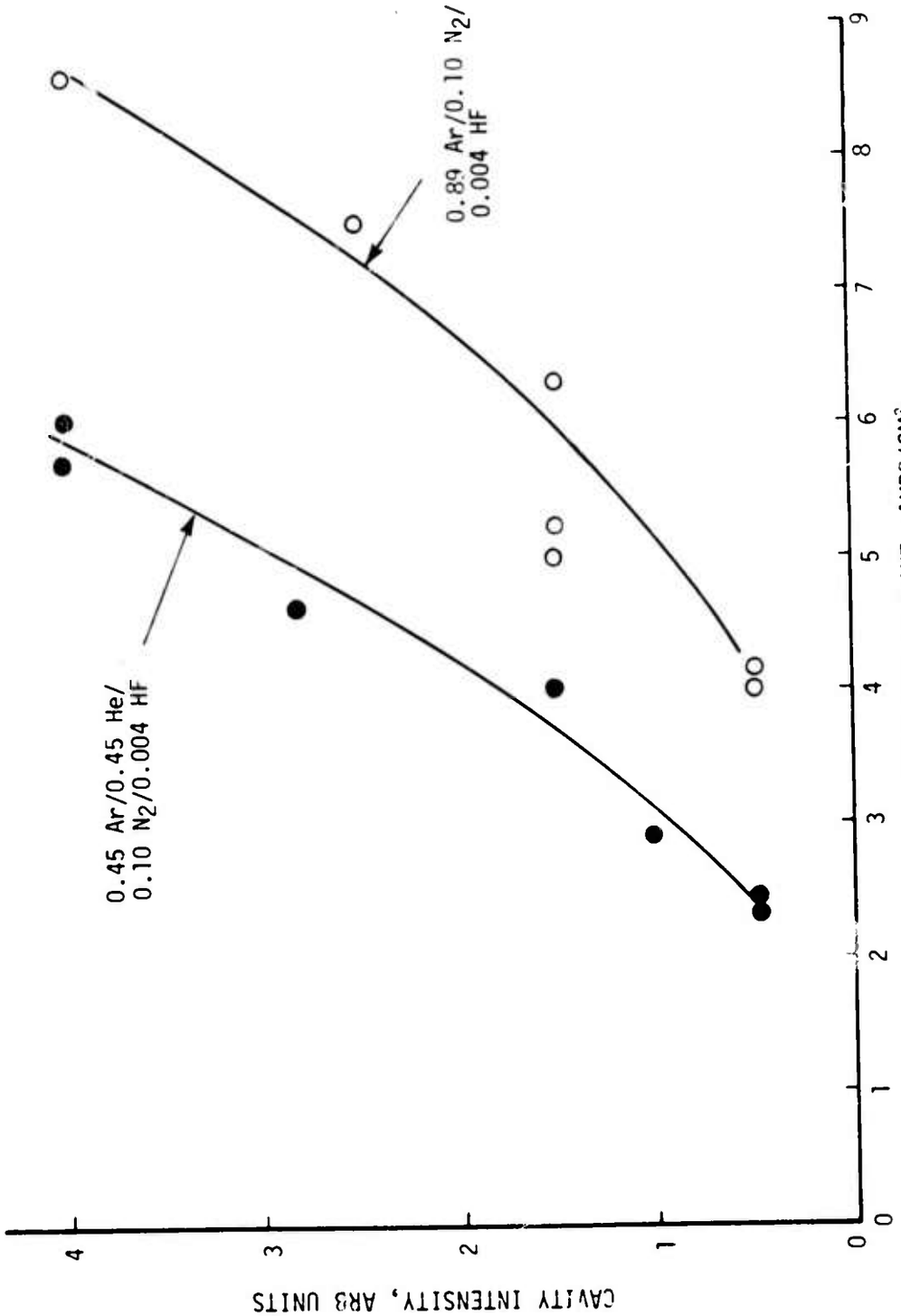

Figure 4. Peak Laser Cavity Intensity in $Ar/N_2/HF$ and $Ar/He/N_2/HF$ Mixtures at 200 Torr, Using E/N Values of 0.7 to 1.0 x 10^{-16} V-cm^2

with 3(b), the addition of helium increased the laser cavity intensity by about a factor of 4 for nearly equal values of E/N and discharge currents in $Ar/He/N_2/HF$ mixtures compared to $Ar/N_2/HF$. The e-beam current was adjusted in order to produce equivalent discharge currents at fixed E/N for this comparison, since the added helium reduces the discharge current for a fixed e-beam current. When the e-beam current was not attenuated by running the plasma diode at low voltages and pressures, about the same cavity intensity was observed in $Ar/He/N_2/HF$ and $Ar/N_2/HF$ (compare Figures 2(b) and (c)). However, it is seen that the $Ar/N_2/HF$ mixture required higher discharge current to achieve the same laser cavity intensity.

The increase in cavity intensity in mixtures containing helium is attributed to rotational relaxation of the HF by helium. Rotational heating of HF by V-R,T decay processes has been observed previously in measurements of vibrational decay of HF (Ref. 2). In those experiments, heavy dilution by argon was required to provide sufficiently rapid rotational relaxation during vibrational decay of HF. In our HF electric discharge laser strong rotational excitation of HF occurs through V-R,T decay and also by direct electron impact excitation of HF rotation. Thus the addition of helium can reduce the HF rotational temperature by increasing the rate of R-T relaxation. This lower rotational temperature would then increase the partial population inversion responsible for laser emission.

2.3. Laser Output Energy Measurements in HF Gas Mixtures

An optical output coupler was added to the high-Q laser cavity (Ref. 1) used in these experiments by introducing a CaF_2 flat between one CaF_2 Brewster angle window and one total reflector. The normal to the CaF_2 output coupler was rotated at various angles in a plane containing the optical axis and the normal to the Brewster window. Thus the output coupling range is from zero at the Brewster angle to a maximum of 12.6 percent at near normal incidence (3.15 percent per surface per pass). With the output coupler at 45 degrees to the optical axis the output coupling is 3 percent, and with the normal at 30 degrees to the optical axis, it is 10 percent.

Output energy measurements were made for $Ar/N_2/HF$ and $Ar/He/N_2/HF$ mixtures using a "rat's-nest" energy meter (sensitivity 0.6 J/mV) having a collecting aperture of 2 cm diameter. For 10 percent output coupling, 11 millijoules output was measured for (89/10/0.3) $Ar/N_2/HF$ at 200 torr. This corresponds to about 0.06 percent of the input discharge energy and an output energy density of about 0.3 J/ℓ-atm. However, an $Ar/He/N_2/HF$ (78/14/7/0.3) mixture under nearly identical e-beam current, discharge voltage, and output coupling gave approximately 65 percent of the output measured without helium. Hence, any effect helium may have on the rotational equilibration of HF (as noted in the previous section) is apparently offset by the reduced discharge current produced by the presence of large helium fractions and/or by an increase in the V-R,T decay of HF caused by the helium.

Laser output measurements were also made for $Ar/H_2/HF$ mixtures (94/5/0.4). Using the same output coupling (10 percent) and energy meter described above, only about 30 percent of the maximum energy measured for $Ar/N_2/HF$ mixtures was obtained. This reduced output energy may be due in part to the nonuniform electric discharge, which produces regions of absorption as well as regions of gain for $Ar/H_2/HF$ mixtures, as shown by the probe laser measurements described in Section III. To overcome the effects of non-uniformity, a uniform, 50 cm long, plasma diode electron beam is being constructed.

2.4. Chemical Laser Output Observed with $Ar/H_2/SF_6$ Mixtures

The laser wavelengths obtained from $Ar/H_2/SF_6$ mixtures (87/10/3) using electron beam excitation were studied since this laser can be operated at the same pressure as the $Ar/H_2/HF$ and Ar/HF lasers and hence would be suitable for probe measurements free of pressure induced line shift problems. The large electron attachment cross section of SF_6 prevented any discharge current from being drawn when an external electric field was applied. Thus only electron beam excitation was used.

The observed lines, using the entire plasma diode are shown in Table II. A typical oscilloscope trace is shown in Figure 5, indicating long pulse laser emission at high pressure (200 torr), which would provide a useful probe laser. A single plasma diode tube was also used to give laser emission; the effective excitation path was only 8 cm.

Table II

Spectroscopic Measurements of Chemical Laser Emission in $Ar/H_2/SF_6$ Mixtures

(Gas Pressure 200 Torr)

Transition V	Transition P(J)	Wavelength, μm	Time Duration (μsec)
2-1	5	2.795	6-16
	6	2.832	13-42
3-2	5	2.926	7-23

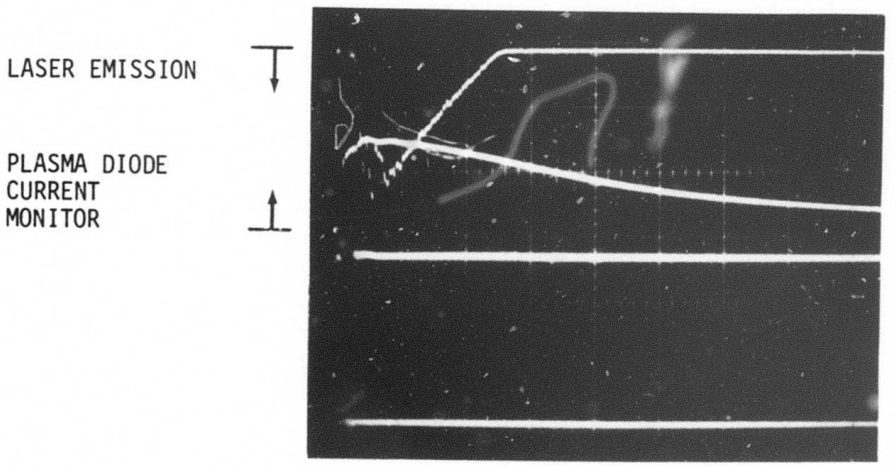

Figure 5. HF Laser Emission on All Lines from $Ar/H_2/SF_6$ Gas Mixtures at 200 Torr Pumped Directly by External Electron Beam Excitation Alone (Time Scale - 20 μsec/div)

Although the chemical laser lines noted in Table II are not the same as those observed in the HF electric discharge laser, it is very likely that a cavity with a grating could be used to select the desired lines, making this a useful probe laser for elevated pressure operation. The signal level from the chemical laser was not high, however, and the optical gain may be too low to accommodate the insertion loss introduced by the use of a grating in the cavity. This approach will be pursued further if it becomes necessary to develop a high pressure probe laser.

SECTION III

HF KINETICS MEASUREMENTS AND ANALYSIS

Time resolved probe laser measurements of HF gain and absorption were made to obtain information on the population of HF vibrational levels. This information was needed to verify the V-V pumping mechanism in the H_2/HF system and to determine the correct pumping mechanism in N_2/HF mixtures. Quantitative information on the V-V and V-R,T rate constants can be obtained by comparing these results with those obtained from the computer model being developed. The following section describes the experimental measurement of gain and absorption, summarizes the initial results that have been obtained and presents some comparisons with computer calculations.

3.1. HF Probe Laser Absorption Measurement Technique

A resistor loaded pin laser (Ref. 3) was used as a probe for the gain and absorption measurements. The pin discharge initiates the HF chemical laser by dissociation of SF_6 which leads to reaction of F atoms with either H_2 or CH_4. Figure 6 shows the optical arrangement used for these measurements. The teflon scatterer in front of the monochromator slit was used to eliminate probe laser beam deflection caused by the heated gases in the e-beam discharge chamber. The effect of this deflection was especially evident for Ar/H_2/HF mixtures, where rotational heating was significant and led to a time dependent index of refraction change in the gas, causing severe

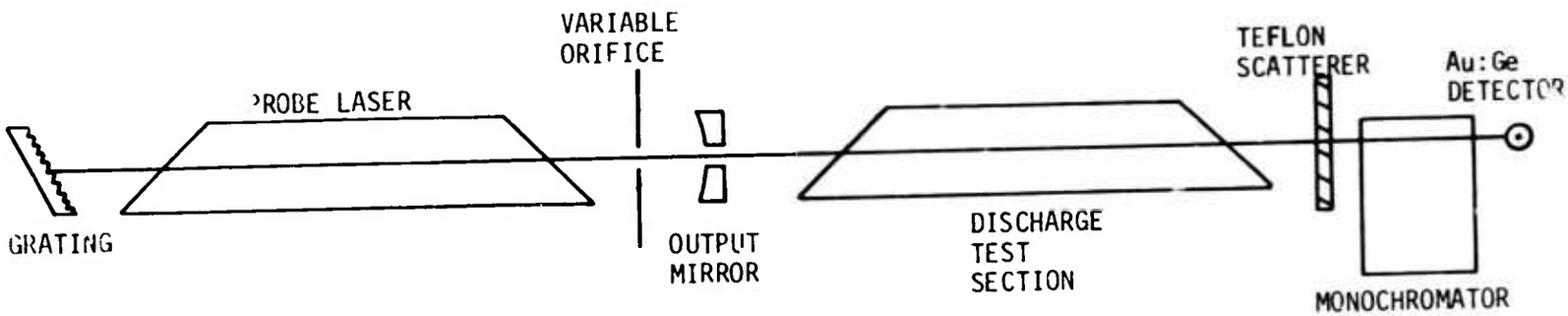

Figure 6. Optical Arrangement Used for HF Probe Laser Absorption and Gain Measurements

deflection of the probe laser beam. The teflon scatterer eliminated signal changes at the detector caused by refractive index changes in the gas, as verified by experiments in Ar/H_2 gas mixtures.

Since the probe laser pulse lasted only about 1 μsec, a series of experiments at one operating condition was required to obtain the time history of the gain or absorption in the long pulse electric discharge laser. The accuracy of the measurement depended principally on the reproducibility of the peak intensity of the probe laser pulse. With a variable orifice aperture in the probe laser cavity to improve shot-to-shot reproducibility, the accuracy realized in these initial measurements was about 10 to 20 percent.

For line selection, a Bausch and Lomb 3.0 μm blazed grating (Blaze Angle 26°45') was used in the probe laser cavity and a ¼-meter Jarrell-Ash monochromator was used just prior to the detector. The cavity grating alone was sufficient to isolate individual HF P-branch transitions on the 1-0, 2-1, and 3-2 bands. For convenience, the monochromator was left in the optical path for checking the wavelength calibration of the cavity grating.

HF concentrations in the test gas mixtures were measured using the P(7) 1-0 absorption line. Figure 7 shows the computed HF (1-0) transmission over the full 82 cm absorption path for different P-branch lines as a function of HF concentration. This measurement permitted reasonably accurate HF concentration determination even at values as low as 0.1 percent.

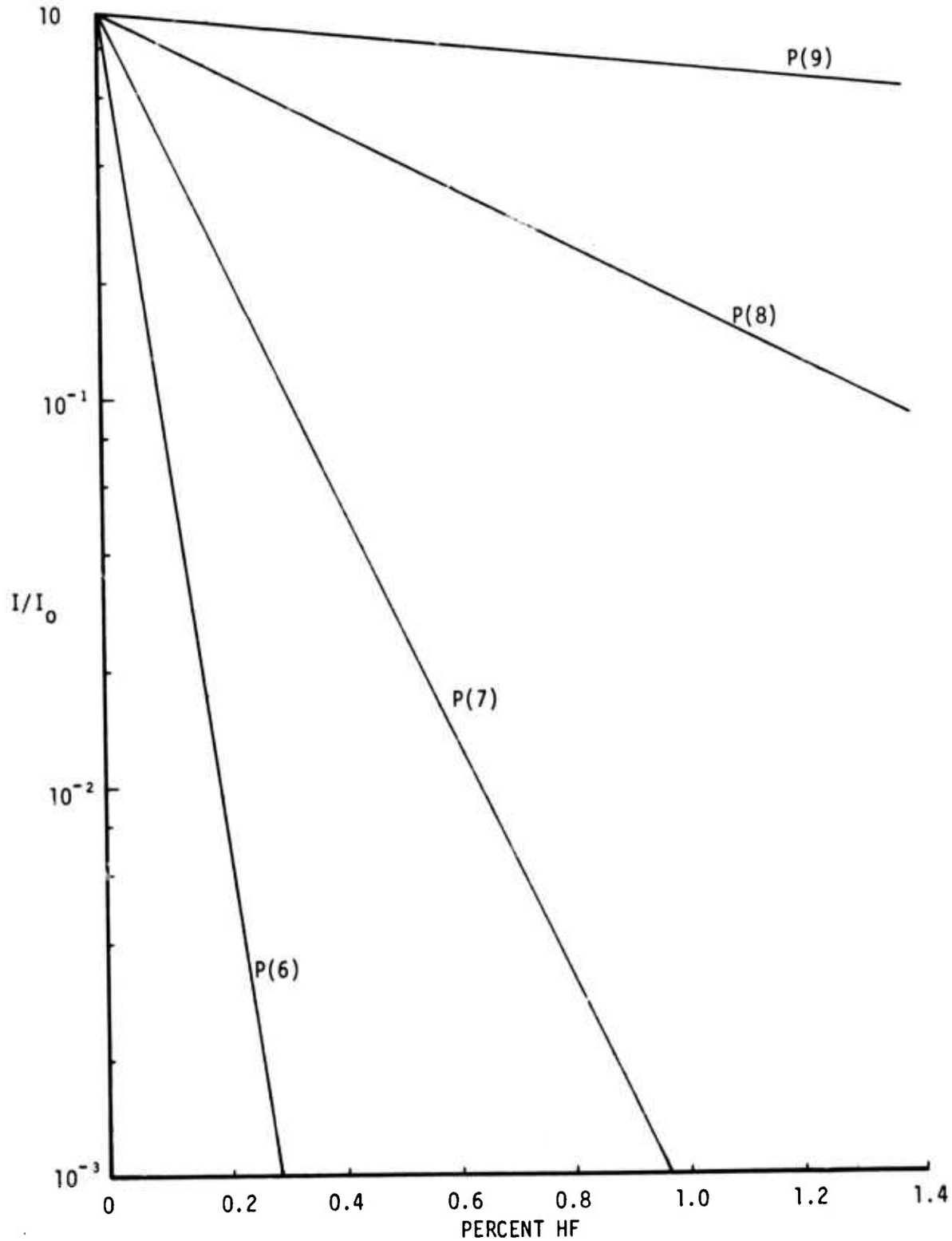

Figure 7. Calculation of HF(v = 0 → 1) Transmission at 300°K and 200 Torr, Heavily Diluted with Ar, Over a Path Length of 82 cm

A serious difficulty, present in all of the absorption and gain measurements given here, is the magnitude of the pressure induced line shift of HF lines in the test gas mixtures relative to the probe laser line center. An approximation is made in all of the measurements discussed here that the shifted absorption coefficient is one-half that at line center in the high pressure test cell at 200 torr (this was discussed in the first semi-annual report (Ref. 4)). A more accurate measurement of this effect will be carried out when a high pressure probe laser is developed.

The probe laser could be fired at any desired time during or after the e-beam sustained discharge by a delay circuit. Typically five probe laser pulses were measured prior to a test; reproducibility of these traces was typically 15 percent. The buildup of gain or absorption was mapped by firing the 1 μsec long probe laser once for each discharge pulse in the test gas, which required several oscillograms to be taken for an adequate time history.

3.2. Probe Laser Absorption Measurements of HF Vibrational Decay

Gain and absorption measurements were made during and after the discharge pulse in HF test gas mixtures. The decay rate following the pulse could be used to evaluate V-V and V-T processes. The populations of the upper HF levels could be used to evaluate the computer model being developed and to determine the temperature rise caused by the discharge.

To obtain vibrational decay rates, absorption measurements were made using the HF probe laser on 2-1 and 3-2 transitions at various time intervals following the crow-bar of the electric discharge. The electric discharge pulse duration was about 30 μsec at current and voltage conditions comparable to those used to produce laser output as given in Section II. Decay rates of the v=1 and 2 levels of HF were then calculated from the e folding time of the absorption decay as the vibrational energy of the gas mixture decayed. Table III summarizes the known HF V-V and V-T rates relevant to the systems investigated and will be referred to in the following discussion.

3.2.1. Ar/N_2/HF Mixtures

The decay curve obtained for a 89/10/0.3 Ar/N_2/HF mixture at 200 torr is shown in Figure 8. From this curve a decay time for HF(v=1) of 21 μsec is obtained, which agrees very well with the V-T decay time calculated (20 μsec) for this mixture using the data of Table III. The rapid decay of HF observed here clearly demonstrates that there is no significant two-quantum N_2 V-V transfer mechanism to pump HF(v) from N_2(v) operating in the Ar/N_2/HF electric discharge laser. Therefore the principal pumping mechanism for Ar/N_2/HF mixtures is direct electron impact vibrational excitation of HF.

Table III

Summary of H_2/HF V-V and V-T Rate Data

Reaction	Rate Constant (a) (sec^{-1} $torr^{-1}$)	Reference
$HF(1) + HF \rightarrow 2HF(0)$	8.7×10^4 (b)	(5)
$HF(1) + Ar \rightarrow Ar + HF(0)$	<60 (b)	(5)
$HF(1) + H_2 \overset{k_{12}}{\rightarrow} HF(0) + H_2$ $H_2(1) + HF \overset{k_{21}}{\rightarrow} H_2(0) + HF$	$k_{21} + 2.6\ k_{12} = 1 \times 10^3$ (b)	(6)
$H_2(1) + H_2 \rightarrow 2H_2(0)$	4.5 (b)	(7)
$H_2(1) + HF \rightarrow HF(1) + H_2(0)$	6.3×10^4 (c)	(5)
$HF(2) + HF(0) \rightarrow HF(1) + HF(1)$	8×10^5	(8)
$HF(3) + HF(0) \rightarrow HF(2) + HF(1)$	1.6×10^6	(8)
$HF(4) + HF(0) \rightarrow HF(3) + HF(1)$	1.4×10^6	(8)
$HF(1) + N_2 \rightarrow HF(0) + N_2$	1.25×10^2	(5)

(a) Rate = $K_{V-R,T} + K_{V-V}$ unless otherwise noted.

(b) Rate = $K_{V-R,T}$

(c) Rate = K_{V-V}

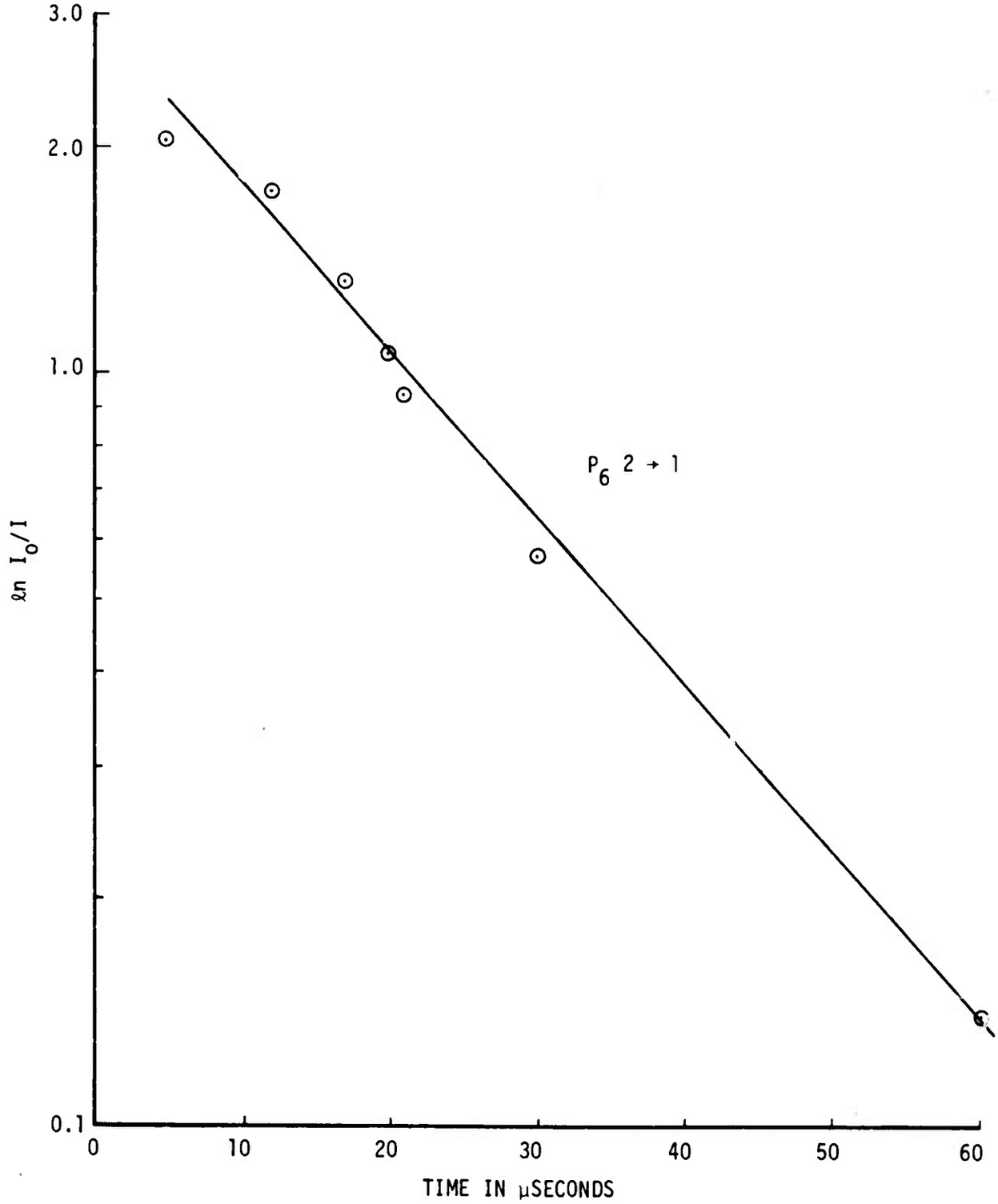

Figure 8. Probe Laser Absorption Measurements of HF(v = 1) Decay Following a 30 μsec Electric Discharge Pulse in 89/10/0.3 Mixtures of $Ar/N_2/HF$ at 200 Torr

3.2.2. Ar/HF Mixtures

The decay curve obtained in a 99.8/0.2 Ar/HF mixture at 200 torr is shown in Figure 9. The short decay time (38 μsec) for HF(v=1) is in agreement with the calculated decay time for this mixture using the rate constants given in Table III. Hence laser action observed for Ar/HF mixtures is due to electron impact pumping of HF, combined with VV ladder climbing as found in CO lasers. In contrast to CO systems, HF self V-R,T deactivation is extremely rapid, and electron attachment to HF is much larger than to CO. For these reasons large HF concentrations probably cannot be used for an efficient electrically excited HF laser system.

3.2.3. $Ar/H_2/HF$ Mixtures

In experiments performed with 89/10/0.3 $Ar/H_2/HF$ mixtures, the decay times are all greater than 100 μsec. This verifies that the V-V transfer mechanism from $H_2(v)$ to HF(v) occurs in the H_2/HF laser. Since the decay time is so long and involves the decay of the combined H_2 + HF vibrational energy, no simple numerical comparisons can be made. The complete computer model, described in more detail in Section 3.3, is required for evaluation and interpretation of these data.

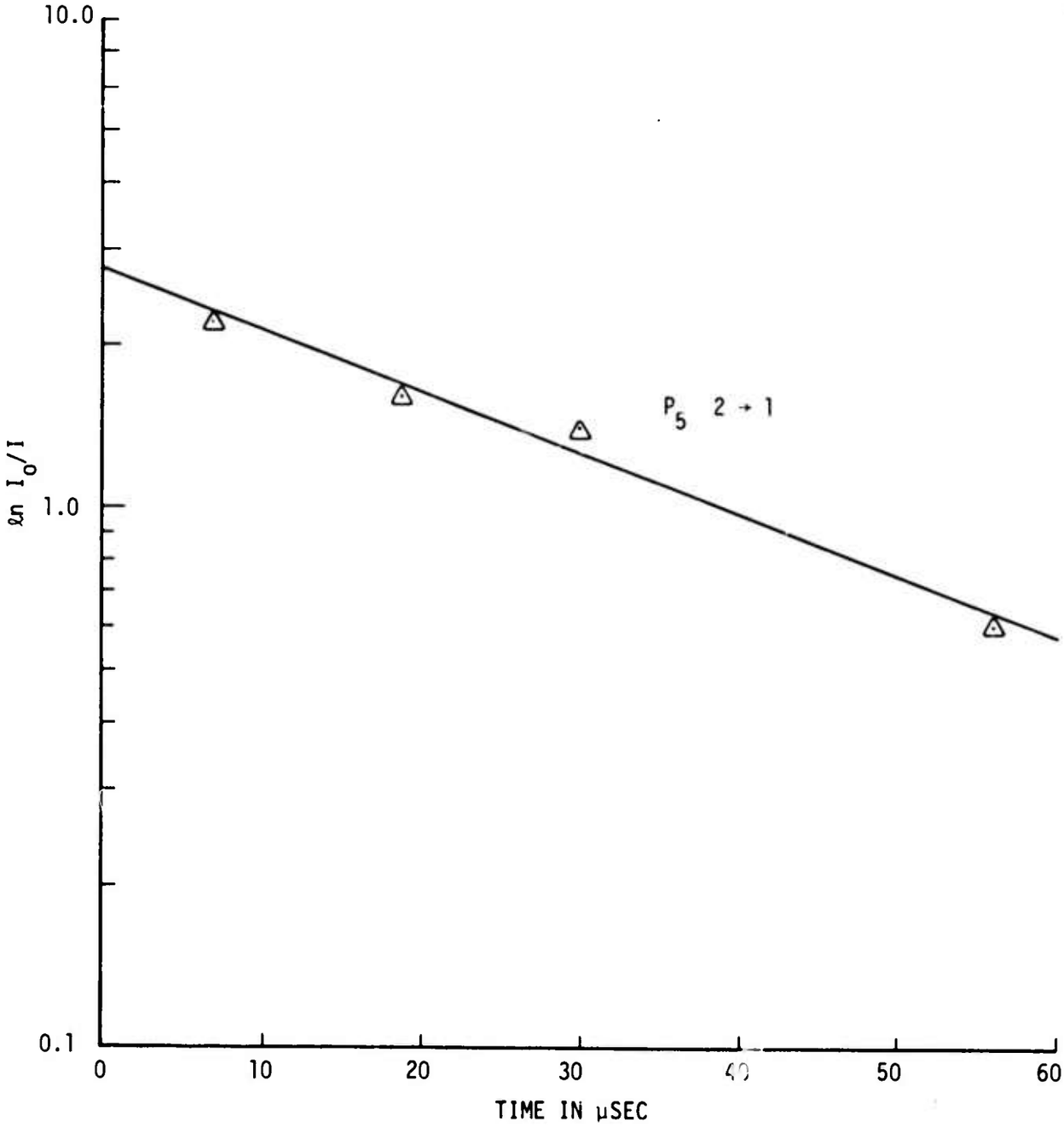

Figure 9. Probe Laser Absorption Measurements of HF(v = 1) Decay Following a 30 μsec Electric Discharge Pulse in 99.8/0.2 Ar/HF Mixtures at 200 Torr

3.3. Comparison of Computer Model with HF Probe Laser Absorption Measurements

Interpretation of the vibrational decay observations in $Ar/N_2/HF$ and Ar/HF mixtures (Section 3.2) is relatively simple and does not require extensive computer modeling. However, interpretation of measurements of the HF vibrational level populations during the excitation pulse and the more complex decay in $Ar/H_2/HF$ mixtures can only be done with the aid of computer modeling. The major elements of the computer model have been described in previous Semi-Annual Reports (Refs. 1 and 4); the specific rate constants and other assumptions used in the present comparisons are given below. Comparisons are made with the results of absorption measurements on the P(5) through P(7) ($v = 2 \rightarrow 1$) probe laser lines for $Ar/N_2/HF$ mixtures and on the P(5), P(6), P(7) ($v = 2 \rightarrow 1$) and P(5) ($v = 3 \rightarrow 2$) lines for $Ar/H_2/HF$ mixtures.

3.3.1. $Ar/N_2/HF$ Excitation Processes

The vibrational decay measurements described in Section 3.2 indicated that the vibrational coupling between $N_2(v)$ and HF(v) is very weak. Thus the electric discharge excitation process occurs primarily through electron impact with HF($v = 0$) to produce $v = 1$ and possibly higher v levels. By carrying out probe laser absorption measurements on several $v = 2 \rightarrow 1$ and $3 \rightarrow 2$ transitions, the $v = 1$ and $v = 2$ populations were determined as a function of time (assuming the rotational temperature remains at 300 °K).

Experimental data are shown in Figure 10 for a 50 μsec electric discharge pulse duration. It is interesting to note that the value of

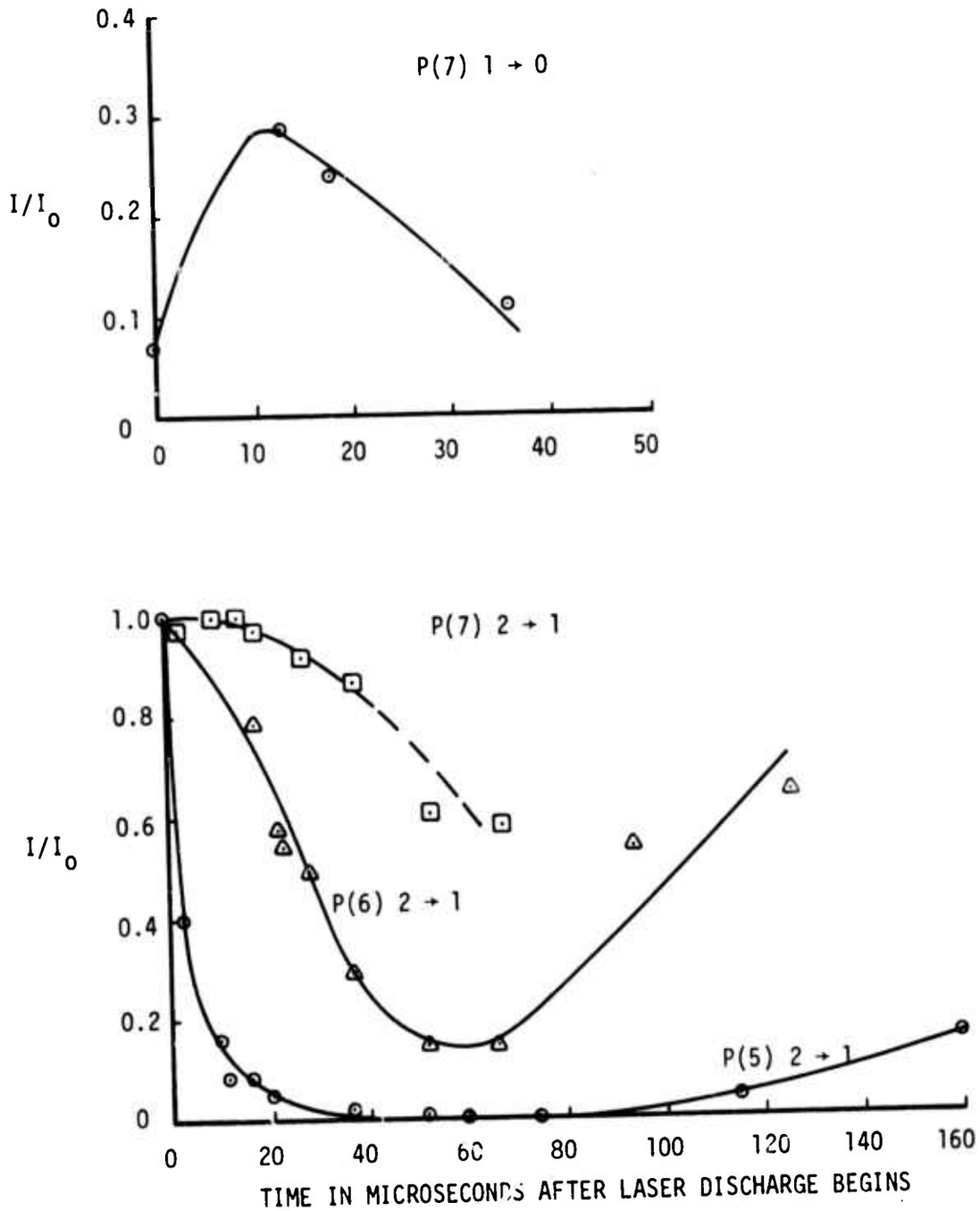

Figure 10. Probe Laser Measurements for a 50 μsec Discharge Pulse in 89/10/0.4 Ar/N_2/HF Mixtures at 200 Torr

the observed minimum in the $P_7(0\rightarrow1)$ absorption at 13 μsec is equal to the value computed on the basis that virtually all of the HF in the 50-cm long electric discharge region is removed by excitation, leaving only a 30-cm long residual absorption path.

Similar experimental data, using a 30 μsec pulse duration, have been reduced to provide populations of the v = 1 and v = 2 levels, as shown in Figure 11. It is seen that the v = 1 and v = 2 populations rise together during the pulse, maintaining a ratio of about 3.7. From the initial slope of the v = 1 population, an averaged cross-section for direct electron impact excitation of HF (v = 0) to HF (v = 1) can be estimated. The electron density is estimated to be 1×10^{13} cm^{-3} on the basis of the measured electric discharge current density (8 amp/cm^2) and an estimated drift velocity of 5×10^6 cm/sec. An excitation cross-section of about 3×10^{-17} cm^2 is computed, assuming that the mean electron temperature is 1 ev and that the average is taken over the range of 0 to 2 ev. This value is comparable with the cross-section for electron impact vibrational excitation of H_2 and may therefore play a significant role in the kinetics of $Ar/H_2/HF$ mixtures.

Attempts to fit the results of Figures 10 and 11 using the present MSNW computer model for HF kinetics and the kinetic data of Table III have not yet yielded satisfactory agreement. However, the initial computations indicate some important trends. A simple model was assumed for the partitioning of electron pumping energy between HF and N_2, with N_2 absorbing 96 percent and HF the remaining 4 percent. This 4 percent was partitioned on a trial basis between direct excitation of v = 1 and v = 2

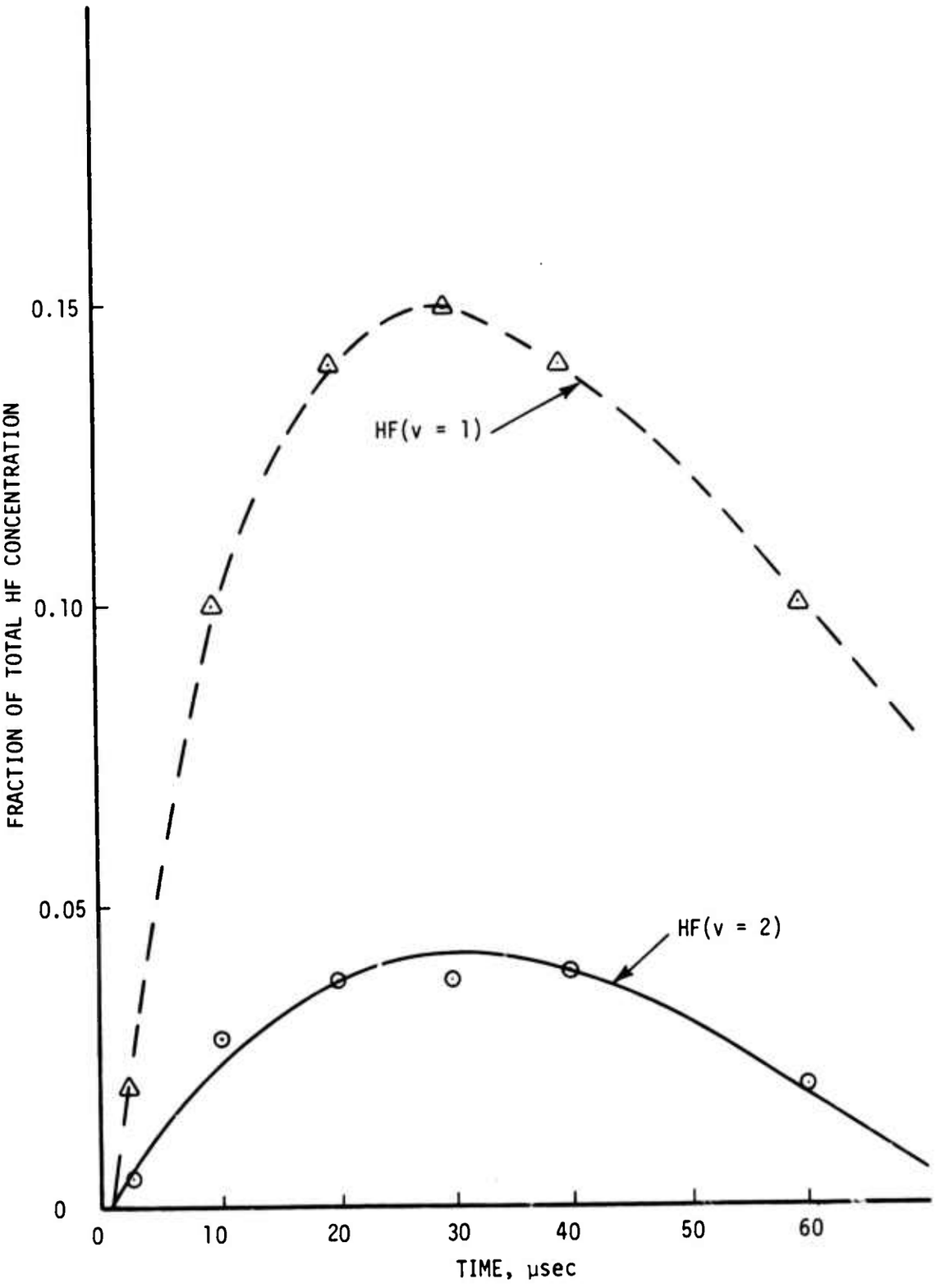

Figure 11. Measured HF Fraction in v = 1 and v = 2 in 89/10/0.4 $Ar/N_2/HF$ Mixtures at 200 Torr Obtained from Data of Figure 10

of HF. Vibrational energy transfer from N_2 to HF was assumed insignificant. The HF rate data of Osgood, Sackett and Javan (Ref. 8), shown in Table III, were used for the upper (v = 2,3,4) HF levels. However, these rates were taken as a sum of k_{VV} and $k_{V\text{-}R,T}$, rather than purely k_{VV}. Rates for the upper level V-R,T processes were then assumed to be equal to either vk_1 or v^2k_1, where k_1 is the HF (v = 1) self V-R,T rate. The corrected V-V rates were obtained by subtracting vk_1 or v^2k_1 from the total rates of Reference 8 . The V-V rates for levels v = 5,6 were taken as gas kinetic.

The computed gain or absorption of the $2 \rightarrow 1$ P(7) transition is shown in Figure 12 for 3 specific cases. Referring back to Figure 10, we note that the measured gain or absorption on this transition was quite small throughout the first 20 μsec of the pulse. This measured value differs from the computer model results that assume electron impact pumping only into the v = 1 level, which show strong absorption at early times. By assuming that HF (v = 2) is pumped at approximately the same power fraction as HF (v = 1), the initial absorption is removed, but strong optical gain is predicted at later times during the pulse, which is not observed experimentally. This latter discrepancy may be due to the fact that very little gas heating was assumed in the computer model. Two conclusions are suggested:

(1) direct electron impact pumping of both the v = 1 and v = 2 levels of HF is significant;

(2) the HF V-V and V-R,T kinetics model does not describe these results satisfactorily.

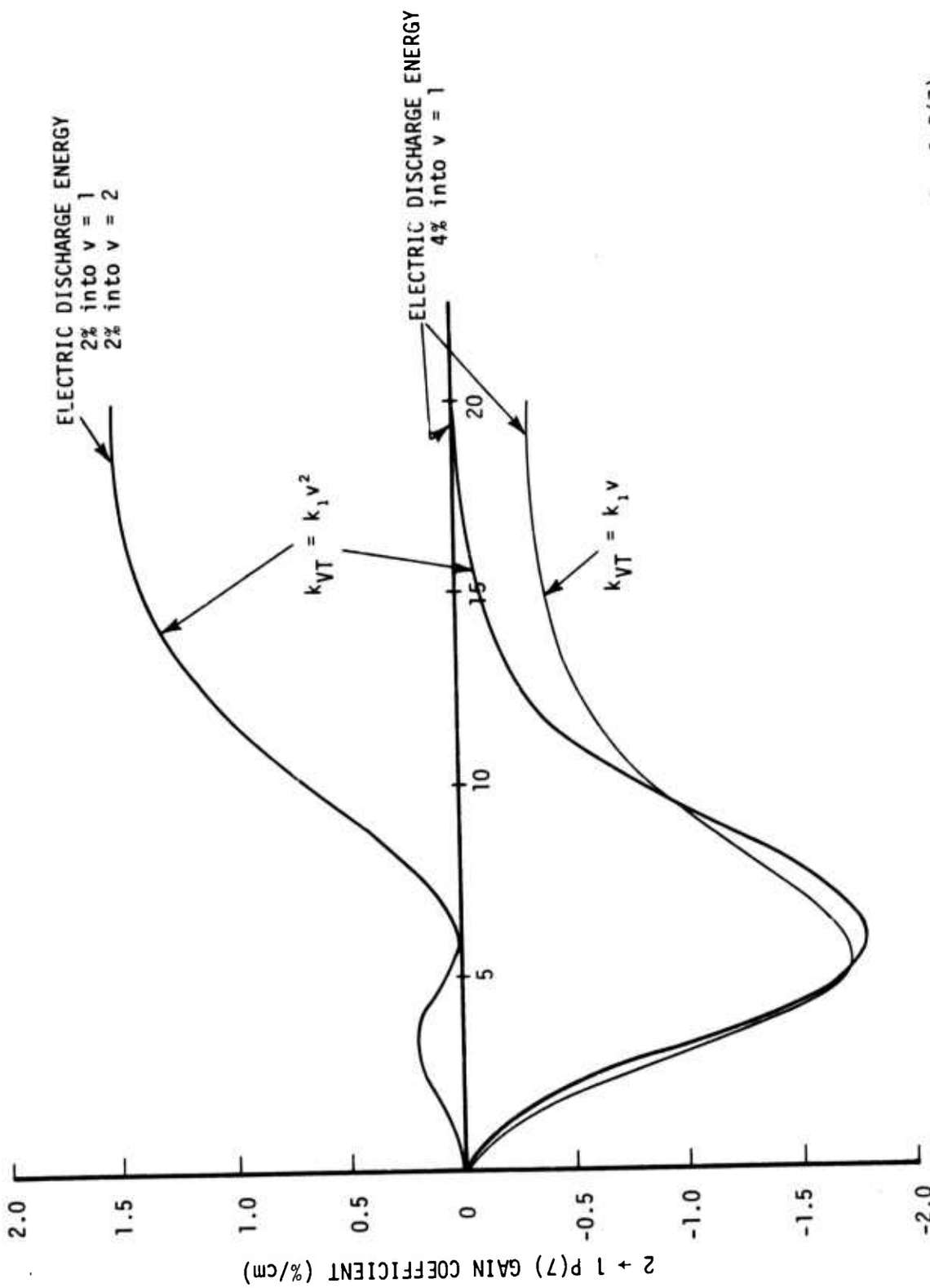

Figure 12. Computer Model Calculations of Optical Gain or Absorption on the 2 → 1 P(7) Transition of HF in 89/10/9.4 Mixtures of $Ar/N_2/HF$ at 200 Torr for a Power Input of 3 kW/cm^3.

3.3.2. Comparison of Computer Model with Absorption Measurements in $Ar/H_2/HF$ Mixtures

Measurements of gain or absorption on the 2 → 1 P(5), P(6) and P(7) and the 3 → 2 P(5) transitions were made in 89/10/0.3 $Ar/H_2/HF$ mixtures at 200 torr using a 30 μsec duration excitation pulse at a power input rate of 1.6 kW/cm^3. The first set of experimental measurements is shown in Figure 13. Gain was not observed at any time on any of the lines studied. This result is consistent with the laser cavity tests made in the same mixture under the same conditions (Ref. 1), which showed no laser emission on the lines monitored in this set of tests.

The MSNW H_2/HF kinetics model was applied to the conditions of these experiments in order to test the model. The basic kinetic information used in the code has been summarized in Table III. In addition, the effects of the following changes in parameters in the model were investigated:

(1) the vibrational dependence of the V-R,T decay rate of HF due to HF collisions was varied as noted in Section 3.3.1;

(2) the temperature dependence of the V-R,T decay rate of HF was included with a T^n law where n was varied between 0 and -2;

(3) the V-V rate of $H_2(v) + H_2(v)$ was varied both in magnitude and in the v dependence;

(4) the V-V transfer rate from $H_2(v)$ to HF was varied both in magnitude and in the v dependence;

(5) the direct electric discharge excitation rate of HF to produce v = 1 and v = 2 was varied;

(6) the uppermost v levels (v = 6) of H_2 and HF were assumed to be excited rapidly to higher levels.

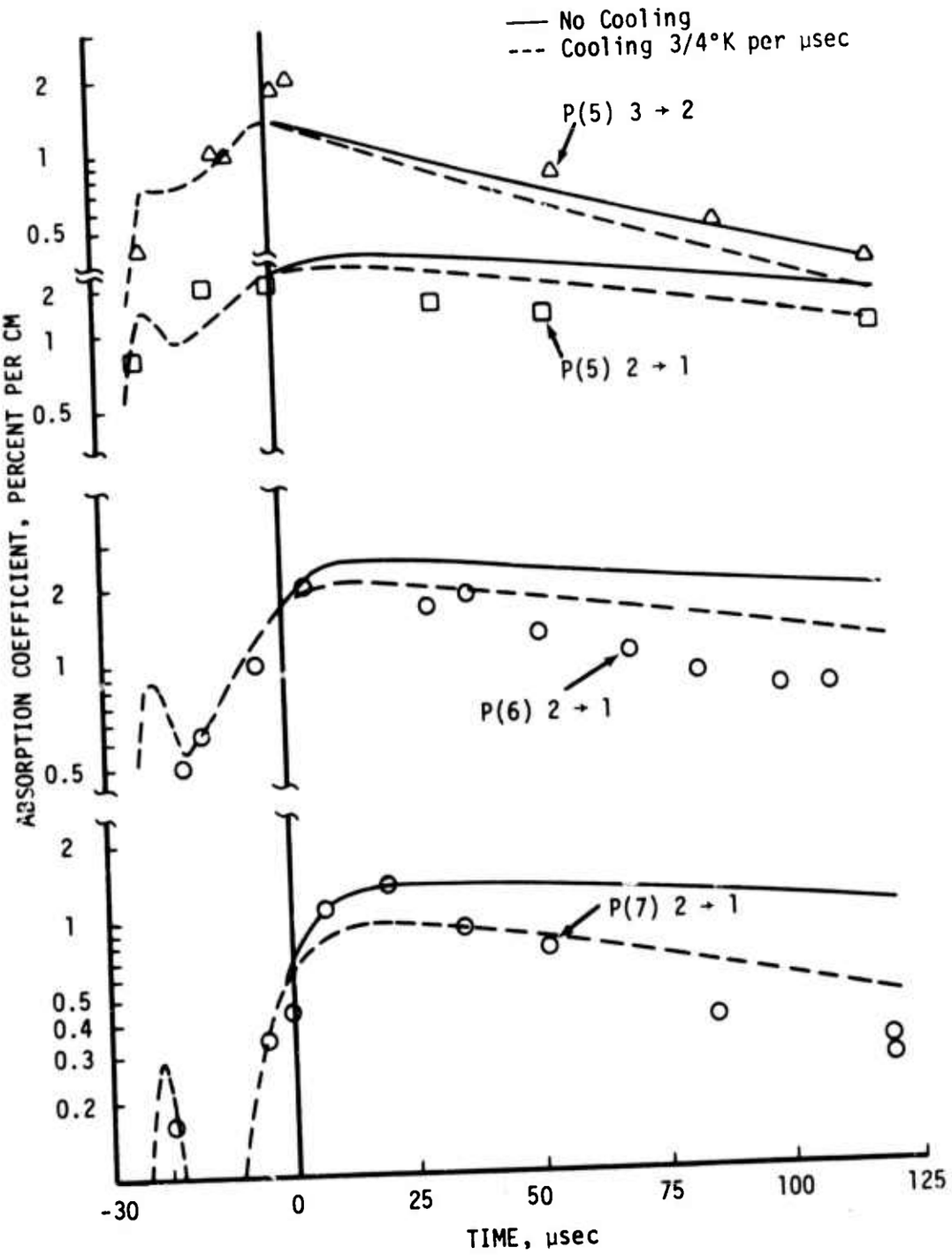

Figure 13. Comparison of Probe Laser Absorption Measurements with Computer Model Results in 89/10/0.3 Ar/H_2/HF Mixtures at 200 Torr and a Power Input of 1.6 kW/cm^3 for 30 μsec

There was no single set of the adjustable parameters that provided a good fit to all of the data. One of the best fits obtained is shown as the solid curves in Figure 13. For this computation, the partitioning of electric discharge energy was the following:

$H_2(v = 1)$ excitation = 0.63

H_2(rot) excitation = 0.27

HF(v = 1) excitation = 0.02

HF(v = 2) excitation = 0.01

direct heating (elastic) = 0.07

In addition, the following kinetic model was used: the HF V-R,T decay rate by HF collisions was assumed proportional to v^2, with a T^{-1} dependence; the H_2 V-V transfer rate among H_2 molecules was based on a probability of 0.002 for v = 1 and was assumed proportional to v; and the $H_2(v)$ transfer to HF(v) was assumed proportional to v.

It is seen in Figure 13 that there is general agreement between the computer model and the magnitude of the measured absorption coefficients; however, important details differ significantly. One of the principal differences is the discrepancy in rotational temperature during the excitation pulse. The $2 \rightarrow 1$ P(7) line is predicted to go into optical gain midway in the excitation pulse, but this is not seen in the absorption measurements nor in the laser cavity measurements. The second principal discrepancy is in the decay following the discharge pulse. The results for $2 \rightarrow 1$ P(5) and $3 \rightarrow 2$ P(5) indicate that the computed decay rate is in fair agreement with experiment. However, the P(6) and P(7) lines of

$2 \rightarrow 1$ indicate a much faster decay than that predicted by the computer model. This suggests a faster cooling mechanism for the gas temperature or the rotational temperature than has been incorporated in the model. The addition of an artificial gas cooling rate (to model expansion cooling) at the rate of 0.75 °K per μsec reduces the discrepancies somewhat as shown by the dashed curves of Figure 13. However, it is concluded that the computer model is not yet satisfactory, particularly in describing the rotational populations of HF. It appears likely that the rotational populations do not fit a Boltzmann distribution and that the transfer of rotational energy to translation is not as fast as assumed in the present model. This possibility is supported by the measured effect on laser output caused by replacing Ar with He, as discussed in Section 2.2.

SECTION IV

ELECTRONIC STATE LASERS: FURTHER STUDY OF THE FIRST POSITIVE AND SECOND POSITIVE BAND SYSTEMS OF N_2

The laser modeling studies described in our previous semiannual technical report suggested the following mechanisms for achieving a long pulse nitrogen laser: 1) pumping of the N_2 (C and B) states by direct electron impact or Ar^* energy transfer; 2) pumping of the N_2 (C) state and removal of the $N_2(A)$ state using the energy pooling reaction ($N_2(A) + N_2(A) \rightarrow N_2(C) + N_2(X)$); 3) selective collisional removal of the $N_2(B)$ state (e.g., by C_2H_6) to eliminate the self-terminating nature of the C → B laser; and 4) use of small concentrations of electronegative molecules such as SF_6 to increase the effective E/N by attaching low energy electrons and thus more effectively pump the N_2 electronic states. These ideas have been tested experimentally during this reporting period and the results are discussed in the following text.

4.1. Experimental Set-Up

It was pointed out in the previous report that the onset of arcing prevented the achievement of the high E/N required for efficient pumping of the N_2 electronic states. In an effort to alleviate the arcing, a new anode with a Rogowski profile at the edges was installed. In addition, the modular design of the e-beam apparatus results in non-uniformities in the discharge, as discussed in Appendix A. These non-uniformities will result in some variation in

the excited state population densities and could represent a serious loss due to absorption of the laser emission. An attempt to correct this problem was made by lowering the discharge screen 4 cm below the e-beam foil. Spreading of the electron beam due to scattering tends to make its profile more uniform at greater distances from the foil; however, the e-beam current density also decreases with distance from the foil, which results in lower discharge current densities.

The rest of the experimental set-up is identical to that used in the HF/DF experiments, with the exception of the mirror coatings and the ultraviolet detector. Gold mirrors were employed for the N_2 first positive cavity tests, and two pairs of dielectric coated mirrors having maximum reflectivities of 99.9% at 3370 Å and 3650 Å, respectively, were used for the N_2 second positive studies. Wavelength selection was obtained with a Jarrel-Ash 0.25 m Ebert Monochromator equipped with both 6000 Å and 2.1 μ blazed gratings. The infrared emission was monitored with an Au:Ge detector while the ultraviolet emission was detected with an RCA 1P28 photomultiplier tube.

4.2. Fluorescence Studies

Time resolved observations of the nitrogen C → B and B → A fluorescence indicate that the C and B states are formed by 1) direct electron impact and/or Ar^* excitation transfer, 2) metastable $N_2(A)$ state self-collisions (energy pooling), and 3) electron impact on metastable $N_2(A)$. Experiments with no applied discharge voltage show

that the N_2 (C and B) states are formed either directly by the e-beam itself, or by energy transfer from Ar^* produced by e-beam excitation. Figure 14(a) is a time history of the nitrogen C → B and B → A fluorescence produced by the e-beam only, while Figure 14(b) shows the effect on these emissions of applying a discharge voltage to the gas. The nonlinear increase in both the 3371 Å and 1 μ emission indicates that the C and B states are formed by some multi-step process, possibly by electron collisions with $N_2(A)$, by collisions between two A state molecules, or by electron impact with excited vibrational levels of ground state N_2.

Another important point to be noticed in Figure 14(b) is that the 3371 Å emission decays with a time constant two orders of magnitude longer than the C state radiative lifetime (~ 40 nsec). This observation suggests that the $N_2(C)$ state is being produced from some long-lived excited species. The most likely candidates are excitation transfer from metastable Ar states or energy pooling by collisions of two metastable $N_2(A)$ molecules. Transfer from metastable Ar atoms can be ruled out on the basis of the measured deactivation rate of Ar^* by N_2. The rate coefficient is 3×10^{-11} cm^3/sec (Reference 9) which, for 20 torr of N_2, implies a transfer time of 50 nsec and an Ar^* decay time of 500 nsec. This is an order of magnitude shorter than the observed decay time.

Whether or not $N_2(A)$ energy pooling is indeed responsible for the formation of $N_2(C)$ should be apparent from the form of the second positive emission decay curve. Loss of the $N_2(A)$ state is controlled by the energy pooling reaction until its population decays sufficiently that quenching predominates. Thus, if the energy pooling

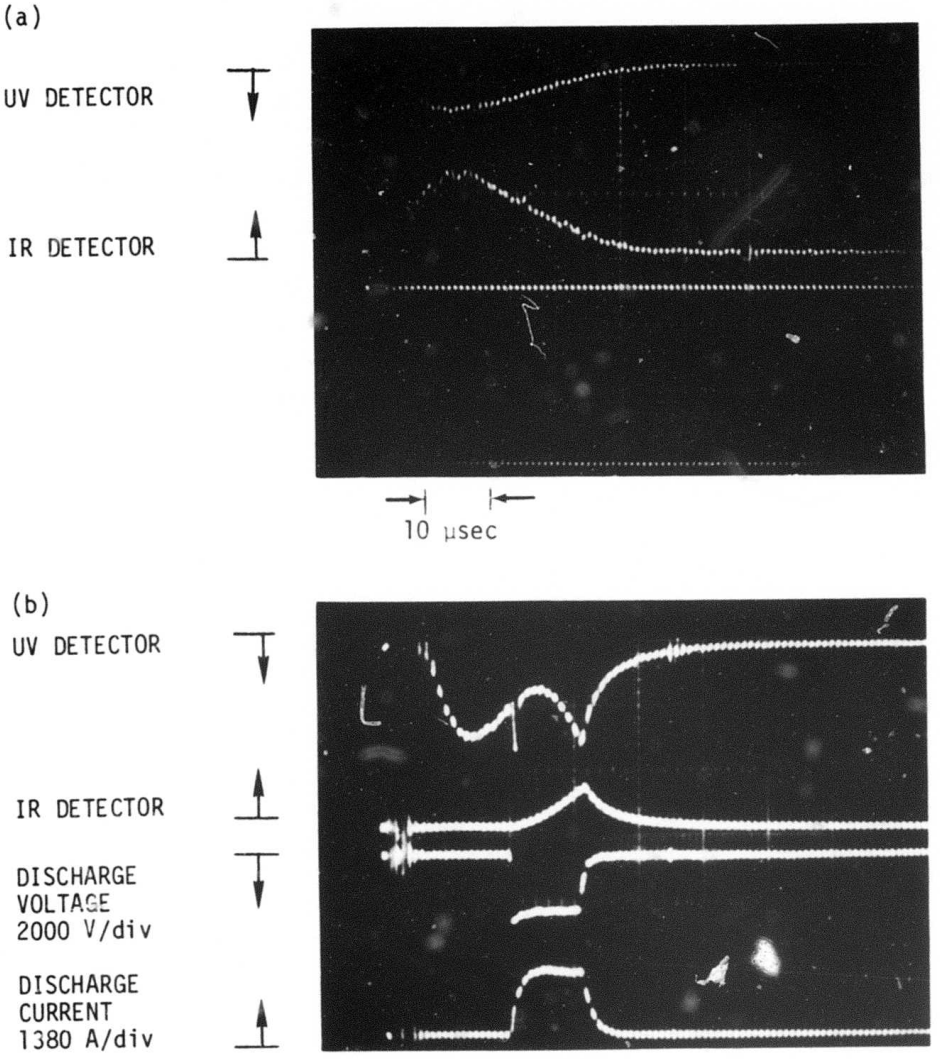

Figure 14. Time History of the Nitrogen C → B (3370 Å) and B → A (1.04 μm) Fluorescence Produced a) by the E-Beam and b) by the E-Beam Stabilized Electric Discharge in an Ar/15% N_2 Mixture at 200 Torr Total Pressure.

reaction which depends quadratically on the A state concentration, is the source of the C state, the 3371 Å emission will exhibit a non-exponential decay. In Figure 15, the intensity of the 3371 Å and 1 μ emission is shown as a function of time after the discharge crowbar. At early times (< 10 μsec) the decay is clearly non-exponential, but at later times it becomes exponential when quenching is the dominant loss process. The similarity between the B and C state decays indicates that there is a close relationship between their populations; the B state is either formed predominantly by radiative cascading from the C state, or it is also formed by A state self-collisions.

If the decay of the $N_2(A)$ state is controlled by self collisions, then it can be described by a differential equation of the form

$$\frac{dA}{dt} = - QA + k_p A^2$$

Here Q is an apparent A state quenching rate constant and k_p is the A state self-annihilation rate coefficient.

The general solution of this differential equation is

$$A = \exp(-Qt)\left[\left(\frac{1}{A_o} + \frac{k_p}{Q}\right) - \frac{k_p}{Q}\exp(-Qt)\right]^{-1}$$

where A_o is the concentration of $N_2(A)$ at time t = 0. At early times (Qt << 1) this solution has the asymptotic form

$$A^{-1} \approx A_o^{-1} + k_p t$$

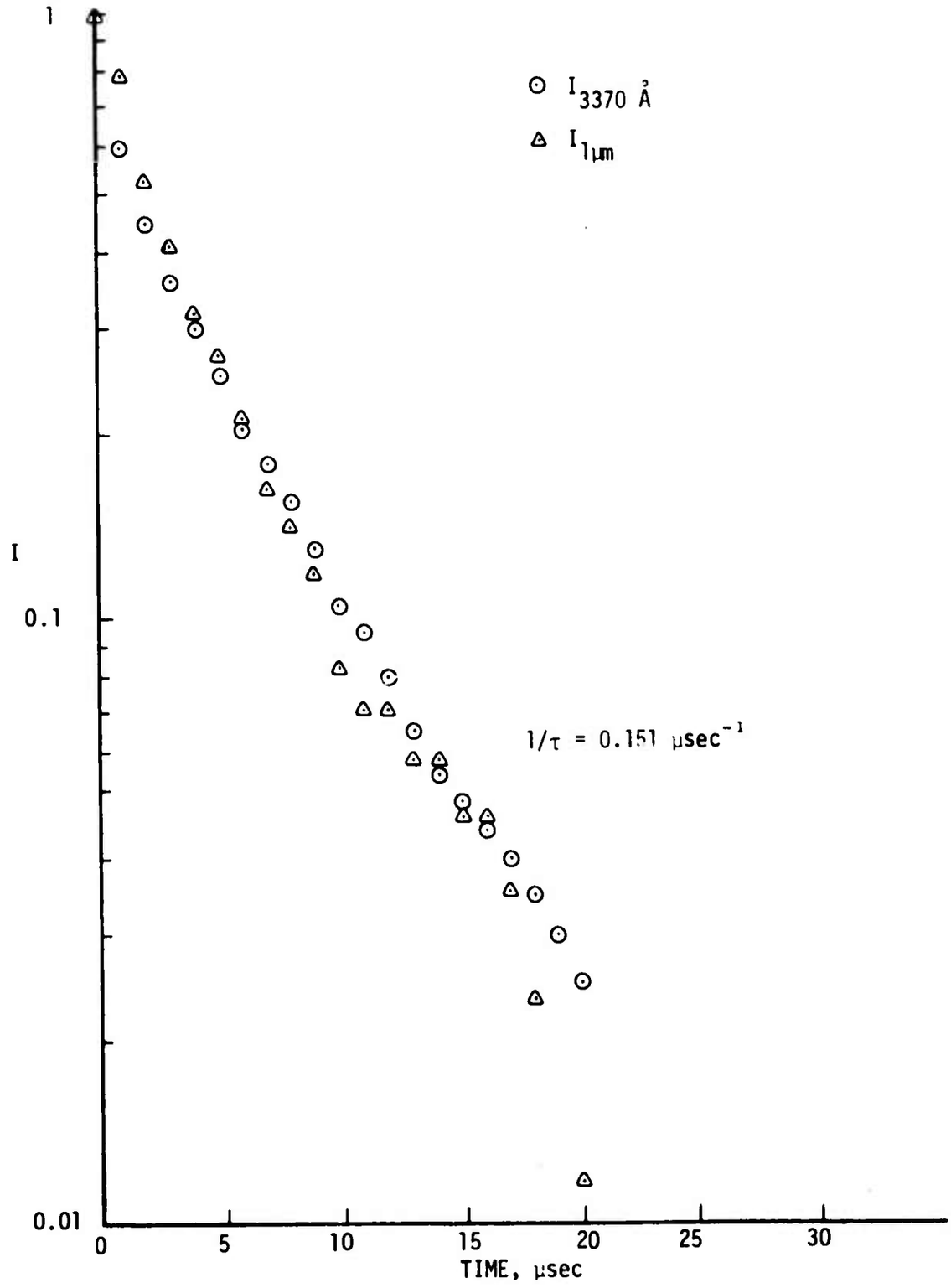

Figure 15. Time Decay of the 3370 Å and 1 μ Emission After the Discharge is Terminated for an Ar/15% N_2 Mixture at 200 Torr Total Pressure

and at late times ($Qt >> 1$)

$$A \sim \exp(-Qt) \left(\frac{k_p}{Q} + \frac{1}{A_o}\right)^{-1}$$

Thus at short times, a plot of A^{-1} vs t should yield a straight line. If the C state is formed from the reaction

$$N_2(A) + N_2(A) \rightarrow N_2(C) + N_2(X) ,$$

then since the C state radiative lifetime is much shorter than its production time, the $N_2(C)$ population should be proportional to $[N_2(A)]^2$ and should have a decay rate equal to twice that of the A state. Hence at short times a plot of $C^{-1/2}$ vs t should also yield a straight line. Figure 16 shows the data of Figure 15 plotted as $I^{-1/2}$ vs t. The linear relationship exhibited by both the C and B state emission implies that the A state decay is indeed being controlled by the energy pooling reaction, and that the energy pooling reaction is the source of the C and B state populations.

From the slope of the exponential decay of $C^{+1/2}$ at long times, it should be possible to estimate the A state quenching constant Q. Since the measured slope scales approximately with the N_2 mole fraction, the A state quenching is more likely attributable to N_2 itself or to some impurity present in or made from N_2 than to Ar or to cold electrons. If the quenching is attributed to N_2 then an approximate rate constant of 8×10^{-14} cm^3/sec is derived from the late time decay of Figure 16. Since the reported values for the quenching coefficient of $N_2(A)$ by

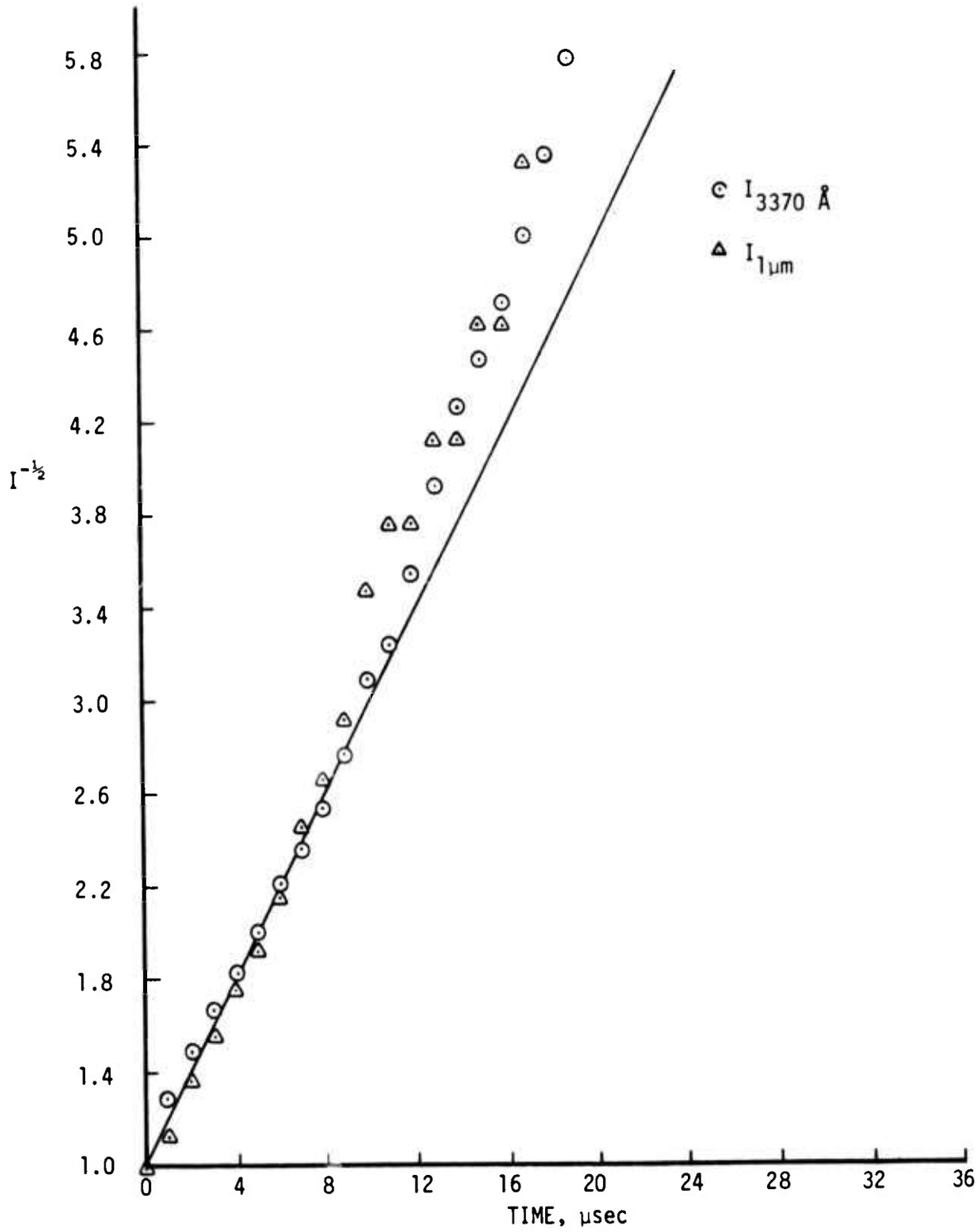

Figure 16. Plot of the Reciprocal of the Square Root of the N_2 First and Second Positive Intensities Versus Time After the Discharge Crowbar

ground state N_2 are $\sim 10^{-16}$ cm^3/sec or smaller (Ref. 10), the A state decay is probably due to an impurity either in the original N_2 storage tank or one produced from N_2 in the discharge. Assuming that it has a gas kinetic quenching cross section for $N_2(A)$, the impurity would constitute $\sim 0.01\%$ of the gas mixture or 0.1% of the nitrogen gas itself.

In a study of Ar/N_2 mixtures excited by a short duration, high-current density pulse of high energy electrons, Eckstrom et al., have obtained similar results for the decay of the N_2 first and second positive emission (Ref. 11). By utilizing the nearly resonant energy transfer reaction

$$N_2(A) + NO(X) \rightarrow N_2(X) + NO(A)$$

and monitoring the NO(A→X) emission they confirmed that there is a close connection between the $N_2(C)$ state and $N_2(A)$ state decays and that at high $N_2(A)$ concentrations self collisions control the decay of the A state population.

Recent rate data indicate that the energy pooling reaction forms the B state approximately four times faster than it forms the C state (Ref. 12). Thus, a C → B laser relying on the energy pooling reaction as the pumping mechanism would be very inefficient. The rate coefficients for the energy pooling reactions as well as for other reactions pertaining to the nitrogen A, B, and C states are listed in Table IV.

It can be seen from the data of Table IV that excitation transfer from metastable $Ar(^3P_{0,2})$ states produces the nitrogen B state 6 times faster than the C state. However, this ratio pertains to the overall

Table IV

Ar + N_2 Excited State Reactions

NO.	REACTION	RATE COEFFICIENT (cm^3/sec)	REFERENCE
EXCITED STATE PRODUCTION			
1.	$Ar(^3P_2)+N_2 \rightarrow Ar+N_2^*$	3×10^{-11}	9
2.	$Ar(^3P_2)+N_2 \rightarrow Ar+N_2(C)$	1.2×10^{-13}	13
3.	$Ar(^3P_2)+N_2 \rightarrow Ar+N_2(B)$	7×10^{-13}	14
4.	$N_2(A)+N_2(A) \rightarrow N_2(C)+N_2(X)$	2.1×10^{-11}	15
		2.6×10^{-10}	12
5.	$N_2(A)+N_2(A) \rightarrow N_2(B)+N_2(X)$	1.1×10^{-9}	12
6.	$N_2(A)+N_2(A) \rightarrow N_2^*+N_2(X)$	1.4×10^{-9}	12
EXCITED STATE QUENCHING			
7.	$N_2(C)_{v=0}+N_2 \rightarrow N_2(?)+N_2$	1.1×10^{-11}	16
8.	$N_2(C)_{v=1}+N_2 \rightarrow N_2(?)+N_2$	2.7×10^{-11}	16
9.	$N_2(B)+Ar \rightarrow N_2(A)+N_2$	1.6×10^{-12}	10
10.	$N_2(B)_{v=0}+N_2 \rightarrow N_2(A)+N_2$	1.6×10^{-12}	17
11.	$N_2(B)_{v=1}+N_2 \rightarrow N_2(?)+N_2$	2.2×10^{-12}	17
12.	$N_2(B)_{v=2}+N_2 \rightarrow N_2(?)+N_2$	3.2×10^{-12}	17
13.	$N_2(B)_{v=3}+N_2 \rightarrow N_2(?)+N_2$	2.5×10^{-11}	18
14.	$N_2(A)_{v=0}+C_2H_6 \rightarrow N_2+C_2H_6$	2.9×10^{-13}	19
15.	$N_2(A)_{v=3}+C_2H_6 \rightarrow N_2(A)_{v\leq 3}+C_2H_6$	1.1×10^{-11}	19

rates for B and C state formation, not to the rates for formation of specific vibrational levels. The results of Setser, et al., (Ref. 14) show that the population of $N_2(B^3\pi_g)v = 3$ resulting from $Ar(^3P_{0,2})$ excitation transfer is more than 15 times less than the population of $N_2(B^3\pi_g)v = 0$. Thus, it still may be possible to obtain an inversion on the $C \rightarrow B(0,3)$ transition utilizing Ar^* excitation transfer as the pumping mechanism.

4.3. Effect of SF_6

At high discharge current densities, the discharge was found to increase the $N_2(B)$ state emission much more rapidly than the C state emission. However, the addition of small concentrations of SF_6 ($\sim$ 0.1%) to the gas mixture increases the ratio of the second positive emission to the first positive emission by an order of magnitude even though the discharge current decreases substantially. The onset of arc formation limited the maximum obtainable E/N to a value of 1.3×10^{-16} V-cm^2 for an 85/15 Ar/N_2 gas mixture at 200 torr total pressure. However, the addition of approximately 0.1% SF_6 to the gas mixture allowed us to achieve an E/N of 2.1×10^{-16} V-cm^2 before arc formation occurred.

The effect of SF_6 addition on the discharge voltage, discharge current, and 3370 Å emission is shown in Figure 17. This photograph should be compared with the oscilloscope traces of Figure 14, which were obtained without SF_6 added to the gas mixture. The discharge E/N in Figure 17 is approximately double that in the shot without SF_6, while the discharge current is about an order of magnitude less in the

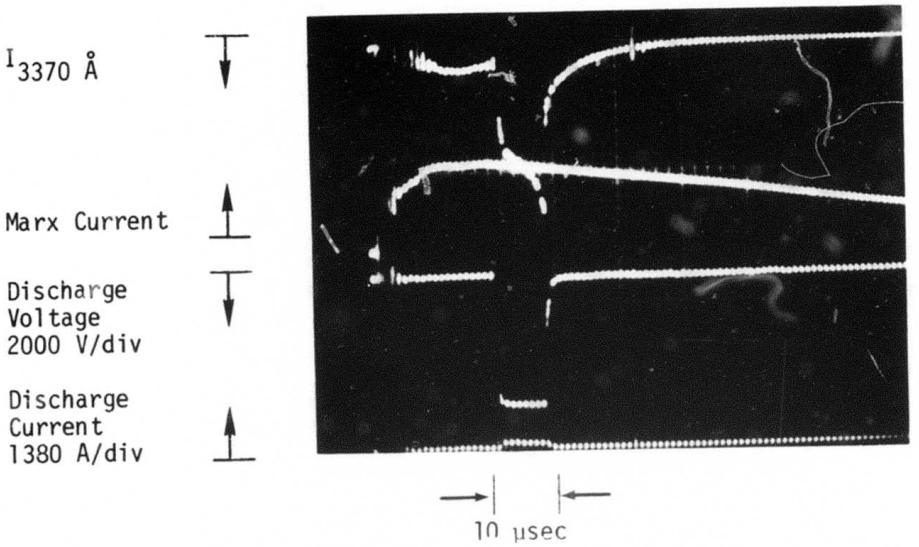

Figure 17. Effect of Approximately 0.1% SF_6 Addition on the Discharge Voltage, Discharge Current, and 3370 Å Emission for an 85/15 Ar/N_2 Mixture

SF_6 case. However, the ratio of the intensity of the 3370 Å emission produced by the discharge to that produced by the e-beam has increased substantially. The abrupt increase of the C → B emission when the discharge voltage is turned on is due to direct electron impact excitation of the C state. The emission then increases non-linearly during the discharge most likely because of the increase in the A state density which populates the C state via the energy pooling reaction. When the discharge is terminated, the second positive emission drops abruptly due to the cessation of electron impact excitation. However, there is still a slowly decaying component to the C state emission after the discharge is turned off. This component is produced by self collisions of the slowly decaying A state population.

4.4. Vibrational Quenching of Lower Level

In our previous report we suggested a collisional decay mechanism for the $N_2(B)$ state utilizing ethane (C_2H_6). This mechanism involved an intersystem crossing from the lower vibrational levels of the B state to the upper vibrational levels of the A state

$$N_2(B^3\pi_g)_{v=0} + N_2 \rightleftarrows N_2(A^3\Sigma_u^+)_{v=7} + N_2 + \Delta E$$

The rate constant for the formation of $N_2(A)v = 7$ reported by Dreyer and Perner (Ref. 19) is $\sim 1 \times 10^{-11}$ cm^3/sec. The $N_2(A)v = 7$ then decays somewhat more slowly down its own vibrational ladder until a bottleneck at the v = 3 and 4 levels is reached. The addition of small concentrations of C_2H_6 increases the rate of decay down the A state vibrational ladder and removes the bottleneck at the v=3 and 4 levels without having a significant effect on the A state electronic energy (see Ref.19).

These ideas were tested by observing the 3371 Å and 1 μ fluorescense with varying concentrations of C_2H_6 as a function of discharge E/N. However, the addition of C_2H_6 did not alter the ratio of second positive to first positive emission. The only observable effect due to the addition of C_2H_6 was the disappearance of the long time decay of both the 3371 Å and 1 μ emission. The apparent implication of this observation is that C_2H_6 removes the A state; however, for the C_2H_6 concentrations used here, this would be inconsistent with the rate constant for electronic quenching of $N_2(A)$ reported by Dreyer and Perner (Ref. 19). One explanation for this inconsistency is that the long time decay component of the first and second positive emission may be formed primarily by energy pooling of A state molecules in higher vibrational levels, which are quenched rapidly by C_2H_6. A second explanation is the formation of other species from C_2H_6 in the discharge, which have a high $N_2(A)$ state quenching rate.

A re-evaluation of the work of Dreyer and Perner revealed an alternate interpretation for the formation of $N_2(A)v = 7$ that is also consistent with their data. The assumption is that the intersystem crossing between the B and A states takes place from the v = 3 level of the B state rather than the v = 0 level. This explanation is also indicated by the factor of ten larger rate coefficient for quenching of the $N_2(B^3\pi_g)$ v = 3 level by ground state N_2 than for the $N_2(B^3\pi_g)v=0,1$, and 2 levels (Ref.18). In fact, the rate constant quoted by Dreyer and Perner (Ref. 19) for formation of the $N_2(A^3\Sigma_u^+)v = 7$ level (9×10^{-12} cm^3/sec) from N_2^* is in better agreement with the N_2 quenching rate constant for the v = 3 level of the B state (2.5×10^{-11} cm^3/sec)(Ref.18) than for the

quenching of the v = 0 level of the B state (1.6×10^{-12} cm^3/sec) (Ref. 17). As a result of this analysis, we now feel that the best candidate for a long pulse C → B laser is the (0,3) band at 4058 Å.

4.5. Laser Cavity Measurements

In an effort to reproduce the superfluorescent emission pulses previously observed in $Ar/N_2/HF$ mixtures for both the first and second positive bands of N_2 (Ref. 4), we searched for laser emission at both 1 μ and 3371 Å when the discharge chamber was placed in a high-Q cavity formed from gold coated spherical mirrors. Even though an E/N of 1.5×10^{-16} V - cm^2 was reached for 89% Ar/10% N_2/1% HF mixtures at 200 torr, no superfluorescent pulses were observed. At present we have no explanation for why we cannot duplicate on our present apparatus the superfluorescent pulses obtained in the old apparatus. One difference between the two experiments is that the e-beam is not crowbarred in the present set up. However, shortening the e-beam pulse by lowering the resistance of a bleeder resistor in parallel with the plasma diode had no significant effect on the first and second positive emission.

Another factor which could conceivably be responsible for the differing results is the size of the discharge volume. In the old apparatus it was 10 cm x 10 cm x 10 cm, and in the present one it is 2.5 cm x 5 cm x 50 cm, which leads us to suspect that radiation trapping (which would be affected by the size of the discharge volume) may have played a role in obtaining the superfluorescent pulses.

High-Q cavity tests using gold coated mirrors and monitoring the 3371 Å emission were made with 85% Ar/15% N_2 gas mixtures both with and without the addition of ∿ 0.1% SF_6. With the addition of

SF_6 an E/N $\sim 1.8 \times 10^{-16}$ V-cm^2 was achieved but no lasing was detected. Mixtures of 85% He/15% N_2 with and without the addition of small concentrations of SF_6 or C_2H_6 were also tested in a high-Q cavity using dielectric coated mirrors having maximum reflectivity at 3370 Å. Again an E/N $\sim 1.8 \times 10^{-16}$ V-cm^2 was achieved, but no optical gain was detected.

Cavity measurements were also conducted with dielectric coated mirrors covering the range from 3500 Å - 3800 Å. This range includes the C → B (0 , 1), (0 , 2), and (1 , 3) bands. Mixtures containing $He/N_2/SF_6$ and $Ar/N_2/SF_6$ at a total pressure of 200 torr were employed. The composition of the mixtures tried and the maximum E/N achieved without arcing are listed below:

Composition	Maximum E/N($\times 10^{16}$ V-cm^2)
69.9% He/30% N_2/0.1% SF_6	3.0
89.9% He/10% N_2/0.1% SF_6	1.7
89.9% Ar/10% N_2/0.1% SF_6	1.7
94.9% Ar/5% N_2/0.1% SF_6	1.4

No laser emission was detected for any of these mixtures.

4.6. Conclusions

The nitrogen B and C states are populated by four mechanisms in the electric discharge: 1) direct electron impact, 2) electron impact with metastable N_2 molecules or with excited vibrational levels of the ground state; 3) metastable-metastable collisions of A state molecules; and 4) Ar^* excitation transfer. Metastable-metastable collisions populate the B state more rapidly than the C state. Excitation transfer from metastable $Ar(^3P_{0,2})$ may create a population inversion on the C → B(0,3) transition.

At high current density, the discharge increases the B state population more rapidly than the C state. Addition of SF_6 tends to stabilize the discharge and increases the ratio of the C to B state emission by an order of magnitude.

Arc formation limits the time during which the high voltage needed to populate the C state can be sustained. The onset of the glow to arc transition needs further experimental and theoretical study to determine the limits it places on electric discharge excitation of electronic states.

A search for laser emission on the $0 \rightarrow 0$(3371 Å), $0 \rightarrow 1$(3577 Å), $0 \rightarrow 2$(3804 Å), and $1 \rightarrow 3$(3755 Å) transitions of the second positive system and the $0 \rightarrow 0$ band of the first positive system was carried out in a high-Q cavity over a range of conditions and gas mixtures. No laser emission was found.

Further review of possible laser mechanisms indicates that the most feasible approach for making a long pulse laser is to utilize electron impact or Ar^* excitation transfer pumping of the C state and collisional quenching of the upper vibrational levels of the B state. A promising candidate for an inversion on the $C \rightarrow B$ transition is the (0,3) band. This is due to an unusually high collisional removal mechanism for the $v = 3$ level of the B state by ground state N_2.

APPENDIX A

PLASMA DIODE CURRENT PROFILES

As pointed out in earlier reports (Refs. 1 and 4), regions of weak HF excitation may lead to absorption coefficients nearly equal to the gain in adjacent regions of a non-uniform discharge. Electron beam current density measurements were made to ascertain the severity of the problem with a five element (1 cm^2 each) Faraday cup array at several vertical positions below the discharge screen cathode. The Faraday cup array could also be moved horizontally along the 50 cm path inside the discharge chamber. The discharge chamber was filled with 90 torr of SF_6 for these experiments. SF_6 has a large electron attachment capability and captures unwanted secondary electrons. In the presence of SF_6 low energy electrons produced in the discharge chamber therefore have a minimum effect on the Faraday cup measurement of high energy electrons.

Figure 18 shows centerline electron beam current density versus distance along the 50 cm horizontal path. The vertical position, 2.3 cm below the discharge cathode screen, is the approximate normal location of the 5 cm x 50 cm discharge anode. Raising the Faraday cup until it is 1.3 cm from the discharge screen increases the peak current density by 40% with little effect on the minimum current density measured between the diode tubes. The large nonuniformities in the electron beam current density profile shown here limit the laser performance that can be achieved, and also cloud the interpretation of the absorption measurements used to obtain information on the excited state populations. A uniform plasma diode gun, 50-cm long, is currently under construction.

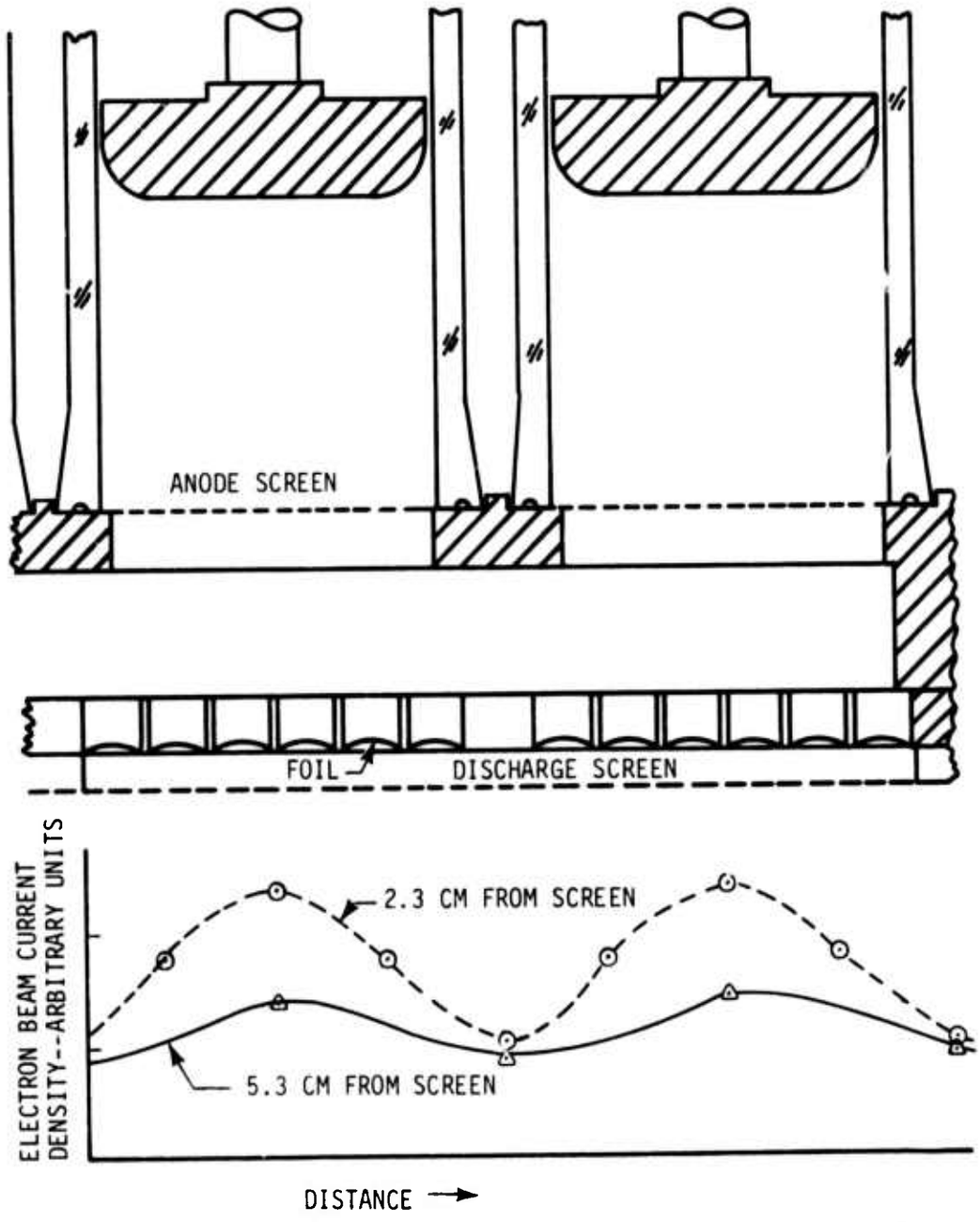

Figure 18. Electron Beam Nonuniformities Measured Below the Foil and Screen of the 5-Tube Plasma Diode Electron Gun

REFERENCES

1. S. R. Byron, et al., Molecular Lasers in E-Beam Stabilized Discharges, Semi-Annual Technical Report No. 2, MSNW Report No. 74-105-2, August 1973.

2. J. K. Hancock and W. H. Green, J. Chem. Phys. 57, 4515 (1972).

3. M. C. Lin and W. H. Green, J. Chem. Phys. 53, 3383 (1970); 54, 3222 (1971).

4. S. R. Byron, Electron Beam Molecular Lasers, Semi-Annual Technical Report, MSNW Report No. 72-105-1, November 1972.

5. J. K. Hancock and W. H. Green, J. Chem. Phys. 57, 4515 (1972).

6. J. F. Bott and N. Cohen, J. Chem. Phys. 58, 4539 (1973).

7. M. A. Kovacs and M. E. Mack, Appl. Phys. Lett. 20, 487 (1972).

8. R. M. Osgood, Jr., P. B. Sackett, and A. Javan, J. Chem. Phys. 60, 1464 (1974).

9. J. LeCalvé and M. Bourène, J. Chem. Phys. 58, 1446 (1973).

10. R. A. Young, G. Black, and T. G. Slanger, J. Chem. Phys. 50, 303 (1969).

11. D. J. Eckstrom, R. A. Gutcheck, R. M. Hill, D. Huestis, and D. C. Lorents, Studies of E-Beam Pumped Molecular Lasers, Stanford Research Institute Report No. MP 73-1, July 1973.

12. G. N. Hays and H. J. Oskam, J. Chem. Phys. 59, 1507 (1973).

13. R. A. Gutcheck and E. C. Zipf, Bull. Amer. Phys. Soc. 17, 395 (1972).

14. D. W. Setser, D. H. Stedman, and J. A. Coxon, J. Chem. Phys. 53, 1004 (1970).

15. D. H. Stedman and D. W. Setser, J. Chem. Phys. 50, 2256 (1969).

16. P. Millet, Y. Salamero, H. Brunet, J. Galy, D. Blanc, and J. L. Teyssier, J. Chem. Phys. 58, 5839 (1973).

17. J. W. Dreyer and D. Perner, Chem. Phys. Letters 16, 169 (1972).

18. H. J. Hartfuss and A. Schmillen, Z. Naturforsch. 23a, 722 (1968).

19. J. W. Dreyer and D. Perner, J. Chem. Phys. 58, 1195 (1973).